

GASKAP—The Galactic ASKAP Survey

John M. Dickey^{1,32}, Naomi McClure-Griffiths², Steven J. Gibson³, José F. Gómez⁴, Hiroshi Imai⁵, Paul Jones⁶, Snežana Stanimirović⁷, Jacco Th. Van Loon⁸, Andrew Walsh⁹, A. Alberdi⁴, G. Anglada⁴, L. Uscanga⁴, H. Arce¹⁰, M. Bailey⁸, A. Begum⁷, B. Wakker⁷, N. Ben Bekhti¹¹, P. Kalberla¹¹, B. Winkel¹¹, K. Bekki¹², B.-Q. For¹², L. Staveley-Smith¹², T. Westmeier¹², M. Burton⁶, M. Cunningham⁶, J. Dawson¹, S. Ellingsen¹, P. Diamond², J. A. Green², A. S. Hill², B. Koribalski², D. McConnell², J. Rathborne², M. Voronkov², K. A. Douglas¹³, J. English¹⁴, H. Alyson Ford¹⁵, F. J. Lockman¹⁵, T. Foster¹⁶, Y. Gomez¹⁷, A. Green¹⁸, J. Bland-Hawthorn¹⁸, S. Gulyaev¹⁹, M. Hoare²⁰, G. Joncas²¹, J.-H. Kang²², C. R. Kerton²³, B.-C. Koo²⁴, D. Leahy²⁵, N. Lo²⁶, V. Migenes²⁷, J. Nakashima²⁸, Y. Zhang²⁸, D. Nidever²⁹, J. E. G. Peek^{30,*}, D. Tafoya⁵, W. Tian³¹ and D. Wu³¹

¹University of Tasmania, School of Maths and Physics, Hobart, TAS 7001, Australia

²CSIRO Astronomy and Space Science, Marsfield, NSW 2122, Australia

³Western Kentucky University, Dept. of Physics and Astronomy, 1906 College Heights Blvd, Bowling Green, KY 42101, USA

⁴Instituto de Astrofísica de Andalucía, CSIC, Glorieta de la Astronomía, E-18008 Granada, Spain

⁵Kagoshima University, Dept. of Physics, 1-21-35 Korimoto, Kagoshima, 890-0065 Japan

⁶University of New South Wales, Department of Astrophysics and Optics, Sydney, NSW 2052, Australia

⁷University of Wisconsin, Department of Astronomy, 475 N Charter St., Madison, WI 53706, USA

⁸Keele University, School of Physical and Geographical Sciences, Keele, Staffordshire ST5 5BG, UK

⁹James Cook University, Centre 101' Astronomy, Townsville, QLD 4810, Australia

¹⁰Yale University, Department of Astronomy, 260 Whitney Ave, New Haven, CT 06511, USA

¹¹University of Bonn, Department of Physics and Astronomy, D-53115 Bonn, Germany

¹²University of Western Australia, Astronomy and Astrophysics, ICRAR, Crawley, W A 6009, Australia

¹³Dominion Radio Astrophysical Observatory, 717 White Lake Rd, Penticton, BC V2A 6J9, Canada

¹⁴University of Manitoba, Dept. of Physics and Astronomy, Winnipeg, Manitoba R3T 2N2, Canada

¹⁵National Radio Astronomy Observatory, P.O. Box 2, Green Bank, WV 24922, USA

¹⁶Brandon University, Dept. of Physics and Astronomy, 270 - 18th St, Brandon, Manitoba R7A 6A9, Canada

¹⁷Universidad Nacional Autónoma de México, Centro de Radioastronomía y Astrofísica, Morelia, Michoacán c.p. 58089, México

¹⁸University of Sydney, CAASTRO, 44 Rosehill St, Redfern, NSW 2016, Australia

¹⁹Auckland University of Technology, Institute for Radio Astronomy and Space Research, 120 Mayoral Dr., Auckland 1010, New Zealand

²⁰University of Leeds, School of Physics and Astronomy, Leeds LS2 9JT, United Kingdom

²¹Université de Laval, Département de Physique, de génie physique et d'optique, Québec G 1 V 0A6, Canada

²²Yonsei University Observatory, Yonsei University, 50 Yonsei-ro, Seodaemun-gu, Seoul 120-749, Republic of Korea

²³Iowa State University, Department of Physics and Astronomy, Ames, IA 500 II, USA

²⁴Seoul National University, Department of Physics and Astronomy, 599 Gwanak-ro, Gwanak-gu, Seoul 151-742, Republic of Korea

²⁵University of Calgary, Department of Physics and Astronomy, 2500 University Drive NW, Calgary, Alberta T2N 1N4, Canada

²⁶Universidad de Chile, Departamento de Astronomía, Camino El Observatorio 1515, Las Condes, Santiago, Cas 36-D, Chile

²⁷Brigham Young University, Department of Physics and Astronomy, N283 ESC, Provo, UT 84602, USA

²⁸University of Hong Kong, Department of Physics, Pokfulam Rd., Hong Kong, China

²⁹University of Virginia, Department of Astronomy, P.O. Box 400325, Charlottesville, VA 22904, USA

³⁰Columbia University, Department of Astronomy, 550 W. 120th St, New York, NY 10027, USA

³¹National Astronomical Observatories of China, Chinese Academy of Sciences, A20 Datun Rd, Chaoyang District, Beijing, China

³²Email: john.dickey@utas.edu.au

(RECEIVED February 10, 2012; ACCEPTED June 21, 2012; ONLINE PUBLICATION January 24, 2013)

Abstract

A survey of the Milky Way disk and the Magellanic System at the wavelengths of the 21-cm atomic hydrogen (H I) line and three 18-cm lines of the OH molecule will be carried out with the Australian Square Kilometre Array Pathfinder

* Hubble Fellow.

telescope. The survey will study the distribution of H I emission and absorption with unprecedented angular and velocity resolution, as well as molecular line thermal emission, absorption, and maser lines. The area to be covered includes the Galactic plane ($|b| < 10^\circ$) at all declinations south of $\delta = +40^\circ$, spanning longitudes 167° through 360° to 79° at $b = 0^\circ$, plus the entire area of the Magellanic Stream and Clouds, a total of $13\,020\text{ deg}^2$. The brightness temperature sensitivity will be very good, typically $\sigma_T \simeq 1\text{ K}$ at resolution 30 arcsec and 1 km s^{-1} . The survey has a wide spectrum of scientific goals, from studies of galaxy evolution to star formation, with particular contributions to understanding stellar wind kinematics, the thermal phases of the interstellar medium, the interaction between gas in the disk and halo, and the dynamical and thermal states of gas at various positions along the Magellanic Stream.

Keywords: Galaxy: evolution, Galaxy: general, ISM: clouds, ISM: general, ISM: molecules, ISM: kinematics and dynamics

1 INTRODUCTION

This paper describes a survey of the Milky Way (MW) Galactic plane, the Magellanic Clouds (MCs), and the Magellanic Stream (MS) that will be carried out at $\lambda\ 21\text{ cm}$ and 18 cm to study the atomic hydrogen (H I) and OH lines. The survey will reach an unprecedented combination of sensitivity and resolution, using the revolutionary phased-array feed (PAF; Chippendale et al. 2010) technology of the Australian Square Kilometre Array Pathfinder (ASKAP) telescope. This telescope is currently under construction in Western Australia by the Australia Telescope National Facility, part of the Commonwealth Scientific and Industrial Research Organisation, Astronomy and Space Science (CASS) branch. The survey described here is among a group selected in 2009 to run during the first 5 years of operation of the telescope. In the longer term, the design and technology used in ASKAP may become the model for the ambitious Square Kilometre Array (SKA) instrument. In the SKA era, surveys like the one described here will advance our knowledge of the Galaxy and its contents in ways that will revolutionise astrophysics. The project described in this paper is a step toward that goal.

The Galactic ASKAP Survey (GASKAP) is the only approved ASKAP project that will have sufficiently high velocity resolution to study the profiles of the H I and OH lines in emission and absorption. It is qualitatively different from the other planned ASKAP surveys in that high brightness temperature sensitivity is the goal for much of the science, e.g. for detecting low column densities of gas. This section describes the strengths of the ASKAP telescope for achieving this goal, and the reasons behind the choice of observing parameters selected for GASKAP. Section 3 discusses some of the scientific applications of the survey data, and the questions it will answer. Sections 4–6 describe the planning for the survey currently underway through simulations, specifications of the data products, and follow-up observations.

1.1 The ASKAP Telescope

The ASKAP telescope (Johnston et al. 2007, 2008) is innovative in many ways, the most revolutionary being its focal plane on which is mounted a PAF and receiver array. As currently designed and tested, the PAF uses no feed horns or other concentrators of the radiation focused by the 12-m

diameter primary reflector. The radiation simply falls on the receiver array, which is carefully impedance matched to minimise reflections and other losses, and contains 188 separate amplifier elements. The signals are then further processed and combined to make up to 36 independent beams with a total area on the sky of 30 deg^2 . Each of these beams acts like the single-dish primary beam of the interferometer, which is made up of 36 dishes and hence 630 baselines. The wide field of view of the small dish-plus-PAF combination leads to a very high survey speed. With only the effective collecting area of a 72-m diameter dish, ASKAP can observe a large area on the sky to a given flux density limit faster than much larger radio telescopes that do not have PAFs.

To detect an unresolved source, the critical telescope parameter is flux density sensitivity, σ_F , which is set merely by the total effective collecting area, system temperature, bandwidth, and integration time (Johnston & Gray 2006). However, for a survey of extended emission that is distributed on angular sizes larger than the synthesised beam, it is brightness temperature sensitivity, σ_T , that matters. For a given total collecting area, the placement of the antennas of the array determines the distribution of baseline lengths and hence both the maximum resolution and the brightness sensitivity. The more widespread the antenna distribution the lower is the filling factor, i.e. the covering factor in the aperture plane, f . Lower filling factor results in worse brightness sensitivity, i.e. higher noise in brightness temperature, σ_T .

The ASKAP telescope is a general-purpose instrument, with baselines up to 6 km in length, but most of the baselines fall in two main groups: one with lengths between 400 and 1200 m and the other between 2 and 3 km (Figure 1). The ASKAP array was designed to provide optimum performance for extragalactic surveys of continuum and spectral line sources, hence the two peaks in the baseline distribution. Fortunately, these two peaks are very well matched to the needs of a Galactic H I survey as well, with the dominant shorter baseline peak giving excellent brightness sensitivity at beam sizes of 30–60 arcsec, while the longer baselines provide higher resolution (10 arcsec) that will allow us to obtain sensitive H I absorption spectra toward continuum sources with flux densities as low as 20 mJy. Similarly, emission from the 18-cm lines of OH occurs both in very compact maser spots and in very widespread but faint thermal emission, while it appears in absorption toward compact, high

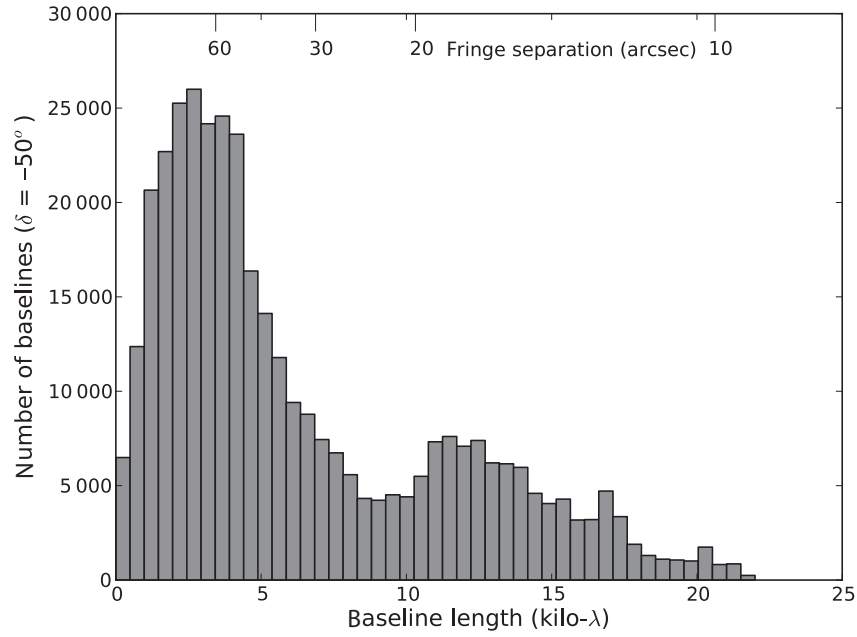


Figure 1. The ASKAP baseline distribution for a source at $\delta = -50^\circ$, from Gupta et al. (2008). The two peaks at 2–6 k λ (0.4–1.2 km) and 10–15 k λ (2–3 km) are designed to optimise the array for both extragalactic spectral line and continuum surveys. For a Galactic survey, they are perfectly placed to measure H I emission and absorption as well as a combination of diffuse OH emission and OH maser emission. The y-axis gives the number of 1-min samples for a source at $\delta = -50^\circ$ in a 10-h observation at 1.42 GHz.

brightness background continuum sources. The ASKAP telescope design is an excellent match to the needs of a Galactic survey of emission and absorption in both the H I and OH lines.

Following Equations (3) and (4) of Johnston et al. (2007), the ASKAP survey speed, $S(\sigma_T)$ in $\text{deg}^2 \text{h}^{-1}$ is a function of the rms noise in the brightness temperature, σ_T , as

$$S(\sigma_T) = \text{FoV} B n_p \left(\frac{\epsilon_c \sigma_T f}{T_{\text{rec}} \epsilon_s} \right)^2, \quad (1)$$

where the field of view (FoV) is 30 deg^2 , the bandwidth B is in Hz, the number of polarisations $n_p = 2$, the correlator efficiency $\epsilon_c \leq 1$, the expected system temperature of the receivers $T_{\text{rec}} = 50 \text{ K}$, the synthesis efficiency given by the taper or weighting of the baselines in the mapping process $\epsilon_s \leq 1$, and the effective aperture filling factor of the antennas is f , where

$$f = \frac{A \epsilon_A N \Omega \epsilon_s}{\lambda^2} \quad (2)$$

with λ being the wavelength in meter, $A = 113 \text{ m}^2$ being the collecting area of a single antenna, $\epsilon_A \simeq 0.6$ being the corresponding aperture efficiency, $N = 36$ being the number of antennas, and $\Omega = 1.13 \theta_s^2$ being the solid angle of the synthesised beam in steradians (sr), where θ_s is the full width at half-maximum (FWHM) synthesised

beamwidth. One of the options for ASKAP resolution has synthesised beamwidth, $\theta_s = 9.7 \times 10^{-5} \text{ rad} = 20 \text{ arcsec}$ (FWHM), giving $\Omega = 1.1 \times 10^{-8} \text{ sr}$, and for the $\lambda 21\text{-cm}$ line $f/\epsilon_s = 5.8 \times 10^{-4}$. Using $B = 1 \text{ km s}^{-1} \simeq 5 \times 10^3 \text{ Hz}$ for the (heavily smoothed) effective bandwidth and $\epsilon_c = \epsilon_s = 1$, the ASKAP survey speed is

$$S(\sigma_T) = 0.10 \left(\frac{\sigma_T}{T_{\text{rec}}} \right)^2 \text{ deg}^2 \text{ s}^{-1} \quad (\text{ASKAP}), \quad (3)$$

and to get sensitivity $\sigma_T = 2.0 \text{ K}$, this gives $S = 0.6 \text{ deg}^2 \text{ h}^{-1}$ corresponding to integration time per pointing of $t_{\text{int}} = \text{FoV}/S = 50 \text{ h}$.

For comparison, the Karl G. Jansky Very Large Array (VLA) C configuration also gives resolution of about $\theta_s = 20 \text{ arcsec}$, but $N = 27$, $T_{\text{rec}} \simeq 37 \text{ K}$ (Momjian & Perley 2011, with $\epsilon_A \simeq 0.6$), $A = 490 \text{ m}^2$, and $\text{FoV} = 0.32 \text{ deg}^2$, resulting in a filling factor $f/\epsilon_s = 1.9 \times 10^{-3}$ and a VLA C Array survey speed of

$$S(\sigma_T) = 1.1 \times 10^{-2} \left(\frac{\sigma_T}{T_{\text{rec}}} \right)^2 \text{ deg}^2 \text{ s}^{-1} \quad (\text{VLA C array}). \quad (4)$$

To get brightness temperature sensitivity $\sigma_T = 2 \text{ K}$ requires $S = 0.12 \text{ deg}^2 \text{ h}^{-1}$, which is about one-fifth the speed of ASKAP.

On the other hand, the Arecibo 305-m telescope with the $N = 7$ multibeam Arecibo L-band Focal-plane Array (ALFA) receiver has $T_{\text{rec}} = 30 \text{ K}$, $n_p = 2$, $\text{FoV} = 3.8 \times 10^{-3}$

deg² for each beam (Goldsmith 2007), and

$$S(\sigma_T) = \text{FoV } B n_p N \left(\frac{\epsilon_c \sigma_T}{T_{\text{rec}}} \right)^2 \quad (\text{Arecibo ALFA}) \quad (5)$$

$$= 270 \left(\frac{\epsilon_c \sigma_T}{T_{\text{rec}}} \right)^2 \text{ deg}^2 \text{ s}^{-1}, \quad (6)$$

or $S = 170 \text{ deg}^2 \text{ h}^{-1}$ for $\sigma_T = 0.4 \text{ K}$ and $\epsilon_c = 1$. Note that the filling factor $f = 1$ for a single-dish telescope with a filled aperture. This survey speed is much faster than any aperture synthesis telescope, but Arecibo's beam size of $\theta_s = 3.5 \text{ arcmin}$ (at $\lambda 21 \text{ cm}$) is far from the 10 arcsec that ASKAP can achieve.

1.2 Survey Description

The GASKAP survey is one of 10 approved survey science projects for ASKAP; its purpose is to study the distribution of H I and OH in the MW disk and the Magellanic System. A summary of the survey areas is presented in Table 1. The GASKAP survey does not seek to cover the entire sky, as single-dish surveys such as Galactic All Sky Survey (GASS) (McClure-Griffiths et al. 2009), Leiden Argentine Bonn (LAB) (Kalberla et al. 2005, 2010), and Galactic ALFA (GALFA-HI; Peek et al. 2011a) have done. The interferometer sacrifices brightness sensitivity for resolution, so the GASKAP niche is to study regions where the emission is bright, but with important structure on small angular scales and narrow velocity widths. H I emission from the Galactic plane and the MCs has brightness temperatures of tens to more than a hundred K, so σ_T of 2 K or less is sufficient to provide good signal-to-noise ratio (S/N). OH masers will appear as bright, unresolved spots of emission; for these the long baselines are needed to maximise the relative positional accuracy at different radial velocities in the same source, thus allowing the precise determination of spatial-velocity structure. High flux density sensitivity is necessary for good astrometry so that OH maser positions can be compared with those of protostellar cores in star formation regions, and with asymptotic giant branch (AGB)/post-AGB stars from optical and infrared (IR) surveys. For H I absorption toward background continuum sources, a resolution of 10 arcsec given by the longer ASKAP baselines will allow the

foreground emission to be subtracted accurately. The optical depth noise is then given by the strength of the continuum and by σ_F , not by σ_T . Thus, the ASKAP telescope provides a great combination of high brightness temperature sensitivity plus high angular resolution that matches the needs of *several different scientific applications*. The scientific objectives of the GASKAP survey are discussed in more detail in Section 3.

To optimise a survey for mapping low surface brightness emission entails matching the telescope baseline distribution to the scale of the structures of interest. For a perfectly smooth brightness distribution, a single-dish antenna is the only tool to use, since interferometers have negative sidelobes that partially or completely cancel out the main beam response, depending on the image restoration technique, e.g. clean or maximum entropy methods (Section 4). GASKAP will depend on supplementary observations with single-dish telescopes to fill in the emission with very large angle structure, corresponding to very short baselines ('short spacing flux'), and ultimately any smooth background ('zero spacing', meaning a brightness constant over the whole sky). The flux sensitivity of an interferometer telescope is calculated by assuming that the source is unresolved, so that even the longest baselines do not suffer any cancellation due to their finely spaced positive and negative sidelobes. The brightness sensitivity can only be calculated given an angular size, using the baseline distribution of the antennas, as in Figure 1. Setting the specifications and strategy of a survey such as GASKAP involves a process similar to impedance matching, where the characteristics of the telescope are optimised for a particular range of spatial frequencies, or angular scales of the distribution of the emission on the sky. For ASKAP, there are relatively few baselines shorter than 100 m, so a single-dish telescope of this diameter or larger is optimum to fill in the short spacings. The Effelsburg Bonn HI Survey (EBHIS) (Kerp et al. 2011) and GASS (Kalberla et al. 2010) surveys will be useful for this purpose.

Any particular interstellar structure, e.g. a shell, cloud, or chimney of whatever shape and size, has a corresponding flux distribution on the u, v plane, given by the Fourier transform of its brightness as a function of position on the sky. The baselines of the telescope should sample this emission on the u, v plane as completely as possible, to give an image

Table 1. Survey Areas

Component Name	Location on Sky (see Figure 2)	Area (deg ²)	Time (h)	Speed (deg ² h ⁻¹)
Low latitude	$ b < 2.5^\circ$, all ℓ for $\delta < +40^\circ$	1650	2750	0.60
Intermediate latitude	$2.5^\circ < b < 10^\circ$, all ℓ for $\delta < +40^\circ$	4890	2038	2.40
Magellanic Clouds	LMC (2) + SMC (1) = 3 deep fields	90	600	0.15
Magellanic Bridge + Stream	$-135^\circ < \ell_{\text{ms}}^a < +66^\circ$, varying b_{ms}^a	6390	2662	2.40
Total		13020	8050	

^aMagellanic Stream coordinates (Nidever et al. 2008); see Figure 3.

of the best possible fidelity, i.e. dynamic range. For a survey, the aggregate distribution of brightness over all angular scales throughout the survey region should be matched by the baseline distribution and integration time of the telescope. For the 21-cm line, the u, v distribution of the brightness in the aggregate follows a power-law function both in the Galactic plane at low latitudes (Crovisier & Dickey 1983; Green 1993; Dickey et al. 2001), in the MCs (Stanimirović & Lazarian 2001), and in the Magellanic Bridge (MB; Muller et al. 2004). The power law is steep, having index -2.5 to -3.5 typically; therefore, given the ASKAP baseline distribution on Figure 1, a reasonable goal for the survey is to obtain σ_T somewhat below 2 K on angular scales of 20 arcsec. On smaller scales, the emission is very faint and the u, v coverage of the telescope is relatively sparse for baselines longer than about 2 km, so very long integration time would be needed to push beyond this sensitivity goal. The longer baselines are useful for absorption spectra toward compact continuum background sources, where brightness sensitivity is not the limiting factor.

Besides the MW and MCs, GASKAP will discover and map the dynamics of dwarf galaxies in the local volume out to Local Standard of Rest (LSR) velocities of $\pm 700 \text{ km s}^{-1}$. Faint, irregular dwarfs typically have narrow Gaussian H I profiles due to their low rotational velocities. Their linewidths are similar to those of high-velocity clouds (HVCs), but their velocity fields are generally very different. Searching for gas-rich, local-group dwarf galaxies is particularly important in the GASKAP survey area at low Galactic latitudes. This science goal overlaps that of the WALLABY project (B. Koribalski et al., in preparation) that will cover the whole sky with a velocity resolution of $\sim 4 \text{ km s}^{-1}$ and 300-MHz bandwidth.

As a pathfinder to the SKA, the frequency range of ASKAP was chosen to be 700 MHz to 1.8 GHz, with a maximum instantaneous bandwidth of 300 MHz. This allows simulta-

neous coverage of the 21-cm line of H I at 1420 MHz and three of the 18-cm OH lines at 1612, 1665, and 1667 MHz, but not the fourth at 1720 MHz. For studies of H I and OH in the MW, MCs, and MS, high velocity resolution is critical. The ASKAP spectrometer provides a total of 16384 channels on each baseline. These will be allocated to a few narrow ‘zoom’ bands with fine velocity resolution. For Galactic observations, a good choice of channel spacing is 976.6 Hz, giving a velocity step of $0.18\text{--}0.21 \text{ km s}^{-1}$ (see Table 2). These narrow spectrometer channels will cover the four lines with LSR velocity ranges of $\pm 760 \text{ km s}^{-1}$ for H I (7394 channels) and $\pm 311 \text{ km s}^{-1}$ for the OH lines (3419 channels at 1612 MHz and 5571 channels covering both the 1665- and 1667-MHz lines together). Since the OH main lines are separated by just 352 km s^{-1} , blending of the two lines is possible in directions where the radial velocity of the emission spreads over more than this amount. This is not expected in the GASKAP survey area. The allowed velocity range due to Galactic rotation in the inner Galaxy, excepting the Galactic Center, covers about -150 to $+150 \text{ km s}^{-1}$ maximum, depending on longitude. In the MCs and MS, the velocity ranges from about $+450 \text{ km s}^{-1}$ in the leading arm (Kilborn et al. 2000) to -400 km s^{-1} (LSR) near the northern tip of the MS.

1.3 Survey Parameters

GASKAP will use three different survey speeds, with integration times of 12.5, 50, and 200 h, which correspond to $S = 2.4, 0.6,$ and $0.15 \text{ deg}^2 \text{ h}^{-1}$. These translate to brightness temperature sensitivities at different angular resolutions as given in Table 3; smoothing to larger beam area gives much lower values of the noise in brightness temperature, σ_T . The flux density sensitivity, given in the last column of Table 3, is only a weak function of angular resolution. The lowest flux density noise level, σ_F , is achieved with resolution 20 arcsec; at this

Table 2. Frequency and Velocity Coverage.

Band	Frequency Range (MHz)	LSR Velocity Range (km s^{-1})	Channel Spacing (km s^{-1})
H I	1416.795–1424.016	± 762	0.206
OH 1612	1610.561–1613.900	± 310	0.182
OH main lines	1663.657–1669.099	± 313	0.176

Table 3. Survey Speeds and Sensitivity.

Survey Component	Map Speed ($\text{deg}^2 \text{ h}^{-1}$)	Dwell Time (h)	σ_T (K), $B = 5 \text{ kHz}$ for θ_{FWHM} (arcsec) =					σ_F (mJy) $B = 5 \text{ kHz}$
			20	30	60	90	180	
Magellanic Clouds	0.15	200	1.01	0.48	0.21	0.12	0.05	0.5
Low latitude	0.60	50.0	2.02	0.96	0.42	0.24	0.10	1.0
Intermediate latitude + MS	2.40	12.5	4.05	1.91	0.85	0.49	0.20	2.0

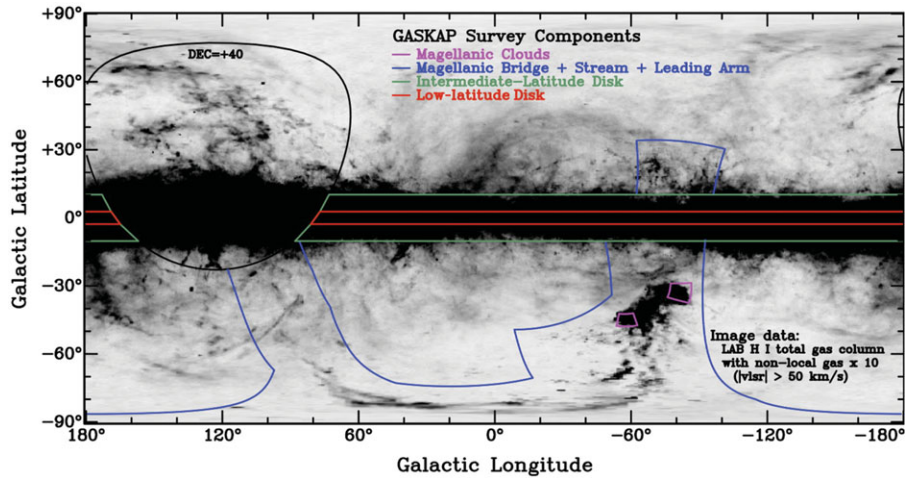


Figure 2. The GASKAP survey areas in Galactic coordinates, with H I column densities from the LAB survey in the background. The region north of $\delta = +40^\circ$ must be filled in from the Northern Hemisphere. The Galactic and Magellanic Emission Survey (GAMES) described in Section 6 will cover the region north of $\delta = +40^\circ$.

resolution all baselines have roughly equal weights ($\epsilon_s = 1$). Just three ASKAP fields are enough to cover most of the area of the MCs, which will have a 200-h integration time per pointing or ‘Dwell Time’ (Table 3, column 3). A single line of 55 fields centered at $b = 0^\circ$ each with a 50-h integration time results in a very sensitive survey of the Galactic plane ($|b| < 2.5^\circ$) over longitudes 167° through 360° (the Galactic Center) to 79° . An intermediate latitude strip of four rows of fields covers $|b| \leq 10^\circ$, centered at $b = \pm 2.5^\circ$ and $\pm 7.5^\circ$. These are observed at the fastest survey speed, with an integration time of 12.5 h on each pointing. Finally, a wide area (about 6400 deg^2) of the MS is covered at the fastest survey speed (12.5 h per pointing). These areas are illustrated in Figures 2 and 3.

2 COMPARISON WITH OTHER SURVEYS

The brightness temperature sensitivity versus angular resolution for the low-latitude GASKAP survey component, which will be observed using the intermediate mapping speed of $0.60 \text{ deg}^2 \text{ h}^{-1}$ (middle row of Table 3), is illustrated in Figure 4, along with the corresponding sensitivities of three recent aperture synthesis surveys of the Galactic plane, the Southern Galactic Plane Survey (SGPS; McClure-Griffiths et al. 2005), the Canadian Galactic Plane Survey (CGPS; Taylor et al. 2003), and the VLA Galactic Plane Survey (VGPS; Stil et al. 2006). Also shown in Figure 4 are the sensitivities and resolutions of the GALFA-HI (Stanimirović et al. 2008; Peek et al. 2011a) seven-beam single-dish survey and the lower resolution, all-sky, EBHIS survey. The GASS survey

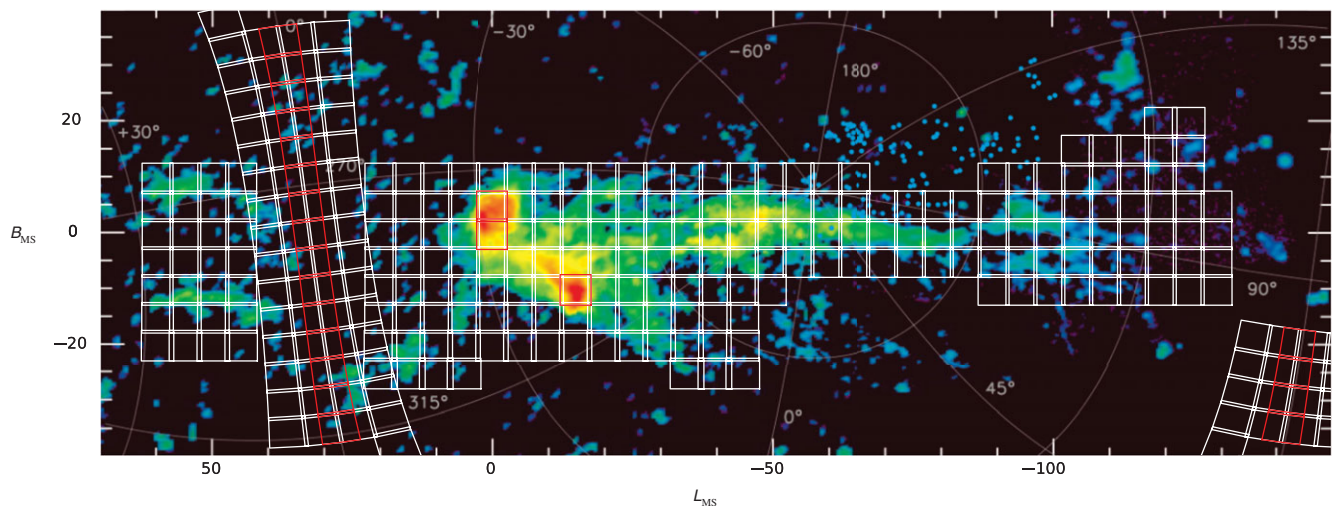


Figure 3. The GASKAP MS survey area with axes labeled in MS coordinates and H I column densities from the LAB survey in the background (Nidever et al. 2010). The white squares represent ASKAP pointings with the shorter integration time (12.5 h), while the red squares are pointings that will be observed for either 50 or 200 h.

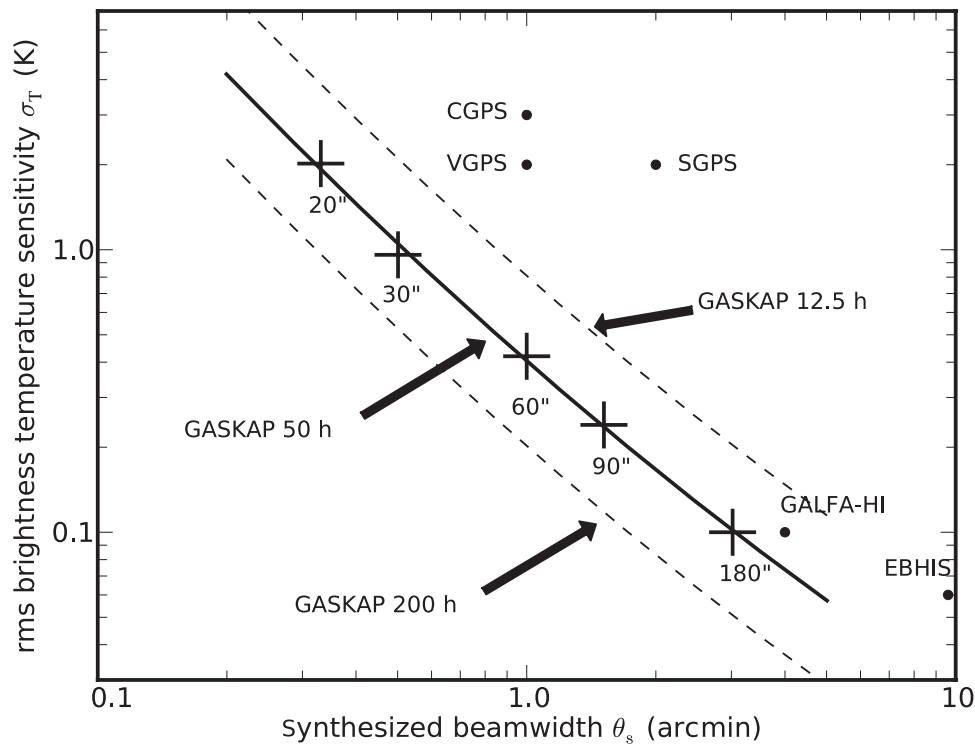


Figure 4. The GASKAP brightness temperature sensitivity (σ_T) vs. resolution (θ_s) with spectra smoothed to 1 km s^{-1} . The solid curve represents the medium integration time of 50 h per pointing, while the other two survey speeds have integration times four times longer or shorter, and hence they have sensitivities a factor of 2 higher or lower, indicated by the dashed lines (see Table 3). On the left ($\theta_s \lesssim 20 \text{ arcsec}$) are combinations appropriate for OH maser emission and H I absorption at low latitudes, and on the right ($\theta_s \gtrsim 1 \text{ arcmin}$) are combinations appropriate for low column density H I in the MS and diffuse OH emission in the Galactic plane. H I emission mapping at low latitudes will make use of resolution from 20 arcsec to 1 arcmin, depending on the brightness and angular scales of the emission in each field. The GALFA-HI point is based on a 10-s integration per beam area, smoothed to resolution $\theta = 4 \text{ arcmin}$.

would be off-scale in the lower right. For GASKAP, the lower angular resolution cubes (1.5–3 arcmin) are obtained from the same data as the high-resolution images by smoothing in the image plane or by tapering more heavily in the u, v (aperture) plane. This taper reduces the effective collecting area of the array ($\epsilon_s < 1$) for larger beamwidths, so that the slope of the line in Figure 4 is not as steep as -2 , as expected from Equations (1) and (2) [$f \propto \sigma_T^{-1}$ with all other quantities fixed in Equation (1), and $f \propto \Omega \propto \theta_s^2$ in Equation (2), but ϵ_s decreases weakly with increasing θ_s]. The GASKAP survey is composed of different surveys done simultaneously; the output data from each one will be useful for a variety of applications that require different combinations of sensitivity and resolution, as indicated in Figure 4 and discussed in Section 3.

The trade-off between resolution and brightness temperature sensitivity apparent in Table 3 is at once the limitation and the great power of an aperture synthesis survey of diffuse emission. For Galactic and Magellanic H I emission, the 30 arcsec and 0.2 km s^{-1} resolutions of GASKAP are a breakthrough, because they provide spectral line cubes comparable with the best images from surveys like those from space-based telescopes in the far-IR (6–40 arcsec from the

Spitzer Space Telescope at 24–160 μm) and submillimeter (5–36 arcsec for the *Herschel Space Observatory* at 70–500 μm). GASKAP data cubes will thus provide a well-matched comparison of H I with interstellar medium (ISM) tracers at IR, millimeter, and submm wavelengths. With this survey, it will finally be possible to obtain images of structures in the atomic (H I) medium with the richness and detail routinely available for the dust and molecular gas.

3 SCIENTIFIC GOALS OF THE SURVEY

This section presents a series of short scientific discussions that motivate the different applications of the GASKAP survey. Because of the versatile capabilities of the telescope and spectrometer, all of these goals are achieved simultaneously with the same observations. For study of the interstellar H I and OH of the MW and Magellanic System, the fine velocity resolution of GASKAP is critical, and even more so for OH masers. As high spectral resolution is what distinguishes GASKAP from the other ASKAP survey projects, the science goals mostly are formulated to take advantage of the narrow spectral channels and high brightness sensitivity that will be obtained.

3.1 Galaxy Evolution Begins at Home

One of the great challenges of modern astrophysics is understanding how galaxies form and evolve. This is intimately connected with the outstanding problem of star formation: as star formation transforms the ISM, adding heavy elements and kinetic energy, it determines the structure and evolution of galaxies. While modern cosmological theories can predict the distribution of dark matter in the Universe quite well, predicting the distribution of stars and gas in galaxies is still extremely difficult (Tasker et al. 2008; Putman et al. 2009; Tonnesen & Bryan 2009). The reason for this is the complex and dynamic ISM: simulations reach a bottleneck on scale sizes where a detailed understanding of star formation, its feedback, and the interaction between galactic disks and halos needs to be included (Stanimirović 2010). To make advances in the area of galaxy formation and evolution, we must begin with our home neighborhood where the physics that drives this process can be exposed and studied in detail.

The GASKAP survey focuses on the generic physical processes that drive galaxy evolution by revealing their astrophysical basis here at a redshift of $z = 0$. GASKAP will provide a new and vastly improved picture of the distribution and dynamics of gas throughout the disk and halo of both the MW and the MCs. The data will provide the image detail and broad range of scale sizes that are essential for a quantitative understanding of the physics of the gas in the MW and MCs, including the effects of radiation, shocks, magnetic fields, and the shapes of the gravitational potentials of the disk and halo. Comparing the mixture of warm, cool, and molecular ISM phases in the MW and the MCs shows the variation of the heating and cooling rates with metallicity, and how these processes affect the star formation rate. The MCs studied with GASKAP resolution in position and velocity will show two entire galactic systems in enough detail to trace the connection between star formation and gas infall and outflow. The specific astrophysical processes accessible to the survey are the initial conditions for star formation and ISM phase transitions, the feedback processes in the ISM, and the exchange of matter between the disk and the halo.

3.2 Feedback Processes—Wild Cards in Galaxy Evolution

Galaxy evolution is largely driven by star formation and the subsequent enrichment of the interstellar gas with heavy elements through red giant winds and supernova explosions. By undertaking an unbiased, flux-limited survey of OH masers in the MW and the MCs, GASKAP will image the gas at both ends of this cycle: the first stages of high-mass star formation and the last evolutionary phases of both the massive (8–25 M_{\odot}) supergiant progenitors of Type II supernovae and the more plentiful low- and intermediate-mass stars, i.e. oxygen-rich AGB stars to planetary nebulae (PNe).

The motion of the gas in the disk and halo traces both stochastic processes such as turbulence and discrete, evol-

ing structures such as chimneys and shells. We will study this motion primarily in H I cubes that show the velocity structure of the diffuse medium, supplemented by more detailed maps of molecular clouds in diffuse OH emission and OH masers in regions of massive star formation. These are the sources of the feedback that stirs up the gas (Ford et al. 2008; Ford, Lockman, & McClure-Griffiths 2010; Dawson et al. 2011b). Clouds of neutral, atomic gas in the MW halo are excellent targets for the GASKAP survey because of its high angular resolution. Several examples have been studied with a resolution of 30 arcsec with the VLA (Pidopryhora, Lockman, & Rupen 2009); on this scale, they show sharp density contrasts that suggest that they are unstable in various ways, particularly to Rayleigh–Taylor fragmentation. Thus, cloud mapping in H I can reveal the evolution and dynamics of the gaseous halo. GASKAP is designed to trace the effects of this feedback throughout the MW disk and lower halo.

3.3 How Galaxies Get Their Gas

How much gas flows in and out of the disk through the halo, how fast does it flow, and what forces act on it along the way? How do halo clouds survive their trip down to the disk? These questions can be studied through H I structure in the MS and HVCs (Putman, Saul, & Mets 2011), which reveals the conditions of the outer halo, and in the disk–halo interface, where the Galactic fountain constantly circulates H I as evidenced by chimneys and H I clouds (Stanimirović et al. 2006; Lockman 2002; Ford, Lockman, & McClure-Griffiths 2010; Marasco, Fraternali, & Binney 2012). In low-mass galaxies, outflows are a determining factor in setting the rate of their gradual chemical enrichment. The 30 Doradus mini-starburst in the Large Magellanic Cloud (LMC) may be responsible for part of the MS, either as source or sink (Nidever et al. 2008; Olsen et al. 2011), and the actively star-forming SMC has a porous ISM from which gas easily escapes, yet it is still extremely gas rich (Figure 5). As outflow and accretion rates are expected to be a dramatic function of galaxy mass, GASKAP's comparison of the disk–halo mass exchange in the MW and the MCs will probe the variability of crucial physical parameters governing the large-scale gas flows in three galaxies of very different masses in the range where these rates are expected to change dramatically.

Cosmological simulations predict that gas accretion onto galaxies is ongoing in the present epoch. The fresh gas is expected to provide fuel for star formation in galaxy disks (Maller & Bullock 2004). Some of the H I we see in the halo of the MW comes from satellite galaxies, some is former disk material that is raining back down as a galactic fountain, and some may be condensing from the hot halo gas (Putman et al. 2009; Brooks et al. 2009).

Just how gas gets into galaxies remains a mystery. The large number of gas clouds clearly visible in the Galactic halo is one potential source. HVCs fall into several distinct populations (Wakker & van Woerden 1991), some associated

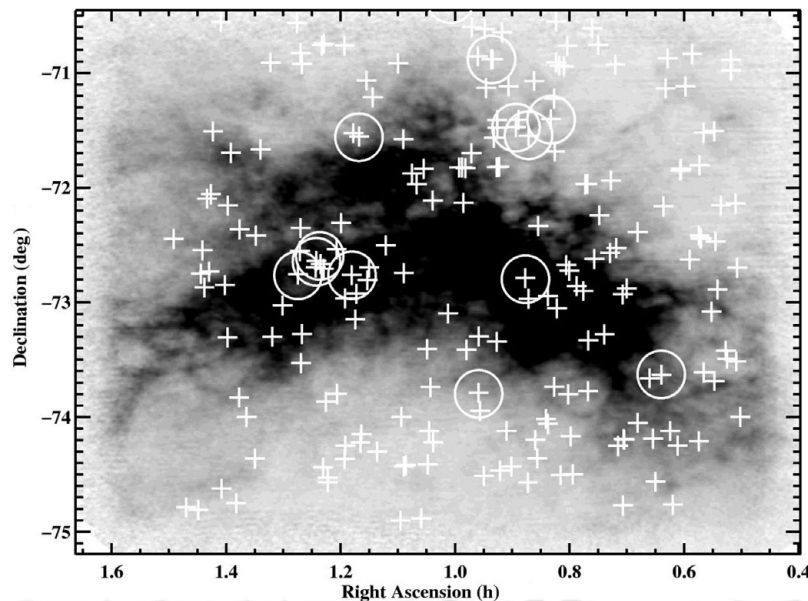


Figure 5. Locations of background continuum sources toward the SMC. The circles show directions for which the H I absorption spectra have already been measured. The crosses show locations of sources bright enough to give good quality absorption spectra with GASKAP.

with the MS and other clouds possibly decelerated by the hot halo (Olano 2008). One exemplar HVC system, known as the Smith Cloud (Lockman et al. 2008), is interesting as a rare example of a fast-moving massive stream ($\sim 10^7 M_{\odot}$) close to the plane of the disk. The Smith Cloud has roughly equal amounts of neutral and ionised hydrogen gas (Bland-Hawthorn et al. 1998; Hill et al. 2009) and appears to have punched through the disk in the last 100 Myr (Lockman et al. 2008). It is difficult to understand how this cloud has survived hitting the disk, or even its passage through the hot halo (e.g. Heitsch & Putman 2009). And yet, if we are to form a complete picture of the life cycle of the Galaxy, it is imperative that we understand how systems like Smith's Cloud and the Magellanic System interact with the Galactic disk.

GASKAP will provide complete, high-resolution coverage of the MS and HVCs associated with its Leading Arm (LA) as well as all HVCs that come within 10° of the Galactic plane. A different ASKAP survey, WALLABY (B. Koribalski et al., in preparation), will complement GASKAP by providing low spectral resolution images of Galactic, as well as extragalactic, H I over the entire sky. The all-sky coverage of WALLABY's Galactic H I component will be useful for tracing full gas streams, such as Smith's Cloud, over large areas of the sky. By working with WALLABY to provide the context, GASKAP will be able to study the processes at work as HVC streams approach the Galactic disk. The spectral resolution of GASKAP will allow measurement of the cooling, fragmentation, and deceleration of H I halo clouds as they near the plane and comparison with models such as those of Heitsch & Putman (2009).

3.4 Disk–Halo Mass Exchange and the Energy Flow in the ISM

For H I emission, the GASKAP survey will provide the biggest improvement over existing survey data in the range 20–90 arcsec with a *tenfold* increase in resolution in most areas. The Galactic plane has been mostly covered at low latitudes ($|b| < 1^{\circ}$ or greater in some regions) by the combination of the Canadian, Southern, and VLA Galactic Plane Surveys (Taylor et al. 2003; McClure-Griffiths et al. 2005; Stil et al. 2006) with resolution ranging from 1–2 arcmin and brightness sensitivity 1.5–3 K rms, and GALFA-HI at 4 arcmin resolution and sensitivity 0.1–1 K rms (Peek et al. 2007). From these surveys we get a hint of the glorious images that GASKAP will produce. The hierarchy of structure and motions of the ISM begins on scales of kiloparsecs, where we see how spiral arms influence gas streaming motions, shocks, and star formation (McClure-Griffiths et al. 2004; Strasser et al. 2007). Continuing to 10–100 pc scales, we see shells, bubbles, and chimneys that trace the collective effects of many supernova remnants and stellar winds (Normandeau, Taylor, & Dewdney 1996; Stil et al. 2004; Kerton et al. 2006; McClure-Griffiths et al. 2006; Kang & Koo 2007; Cichowolski et al. 2008). Moving down to scales of 1 pc and smaller reveals tiny drips and cloudlets in shell wall instabilities (McClure-Griffiths et al. 2003; Dawson et al. 2011a, 2011b), small-scale structure formed in colliding flows in the turbulent disk ISM (Vázquez-Semadeni et al. 2006; Hennebelle & Audit 2007) and ram-pressure interactions between HVCs and the hot Galactic halo gas (Peek et al. 2011a).

Some recent H I detections in dust shells around AGB and post-AGB stars mapped by the Infrared Space

Observatory (ISO) (e.g. Libert, Gérard, & Le Bertre 2007) indicate that GASKAP could provide a larger catalogue of such shells. Considering that the distribution of PNe in height above the midplane, Z , follows that of the OH/IR stars (e.g. the Macquarie/AAO/Strasbourg $H\alpha$ catalogue (MASI-I) catalogue; Miszalski et al. 2008), many PNe will be found at intermediate Z heights (0.3–1.0 kpc above the plane) and so separated from most of the disk gas in the spectrum, and hence their shells may be detectable in H I. The interaction of stellar winds and supernova remnants with the ISM drives interstellar turbulence, seen in the ionised, neutral, and molecular phases with very similar spatial power spectra (Lazarian & Pogosyan 2000, 2006; Haverkorn et al. 2006). The GASKAP data will allow the power spectra of the ISM turbulence to be measured in a variety of different environments, with greater precision, and over a broader range of scales than any survey of neutral gas has done before.

3.5 Phase Changes in the Gas on Its Way to Star Formation

What is the relationship between the atomic and molecular phases of the ISM in different interstellar environments? GASKAP will trace these phases through H I emission, H I absorption, and diffuse OH emission. Comparing them over a large area that contains many kinds of clouds, some forming stars and some not, will show how and where the gas makes the transition from one phase to another. How does the temperature of the gas vary, and how are the different thermal phases mixed in different interstellar environments? GASKAP will investigate this by comparing emission and absorption spectra to measure the excitation temperatures of the H I and OH lines.

In H I absorption, GASKAP will be an even greater advance over existing surveys than it is in H I emission. We expect four extragalactic continuum sources per deg^2 with a peak flux density, F , of 50 mJy or greater, and 10 sources per deg^2 with $F > 20$ mJy (Condon & Mitchell 1984; Petrov et al. 2007). This is at least a factor of 5 more absorption spectra at this noise level than in any previous low-latitude survey. The rms noise is $\sigma_F \simeq 1$ mJy in a spectral channel of width $\delta\nu = 1$ km s^{-1} in the low-latitude survey area. This gives optical depth noise of $\sigma_\tau \leq 0.02$ in the absorption spectrum toward a source with $F = 50$ mJy. These spectra will have excellent S/N in absorption. The more abundant, fainter continuum sources will give absorption spectra of lower quality (e.g. $\sigma_\tau = 0.05$ for $F = 20$ mJy) that will be useful for statistical studies of the cool gas distribution, either by co-adding many spectra or by integrating over velocity intervals much broader than 1 km s^{-1} .

The big question that the absorption spectra will help answer is how the thermal interstellar pressure, which changes by several orders of magnitude from the midplane to the lower halo and from the inner Galaxy to the outer disk, determines the mixture of warm and cool H I (Wolfire et al. 1995, 2003). Combining 21-cm absorption and emission spectra

allows the excitation temperature and column density at each velocity to be measured separately, giving a good estimate of the kinetic temperature. The ambient pressure is tied to the equilibrium temperature through the cooling function of the H I (Field, Goldsmith, & Habing 1969; Dalgarno & McCray 1972). Separating the emission and absorption spectra requires good angular resolution to allow the emission to be measured very near to the continuum source. The highest resolution of the ASKAP array, 10 arcsec, will be excellent for eliminating confusion due to small-scale variations in the emission. Absorption-line studies with GASKAP will be very valuable for understanding the huge range of physical conditions now being found in the neutral ISM (Jenkins & Tripp 2011; Peek et al. 2011b). As an example, Figure 5 shows the level of improvement GASKAP will make relative to previous studies of absorption in the Small Magellanic Cloud (SMC). Only a handful of H I absorption measurements exists for both the SMC and the LMC. White crosses in Figure 5 show the location of radio continuum sources behind the SMC suitable for absorption measurements with GASKAP, while the white circles show what has been done previously by Dickey et al. (2000).

The H I absorption spectra toward continuum sources that GASKAP produces will yield a rich set of gas temperature, column density, and velocity measurements over most of the Galaxy. Matched with these will be complementary, contiguous maps of the cold H I structure and distribution from H I *self-absorption* (HISA) against Galactic H I background emission (Gibson et al. 2000; Gibson 2010). HISA arises from H_2 clouds as well as dense H I clouds actively forming H_2 , so it directly probes molecular condensation prior to star formation (Kavars et al. 2005; Klaassen et al. 2005). A cloud's age can be estimated by comparing its HISA and molecular content with theoretical models (Goldsmith et al. 2007; Krčo et al. 2008). GASKAP's low-latitude survey will easily map the HISA from a 10–20 K cloud with $N_{\text{HI}} > 3 \times 10^{18}$ cm^{-2} . This sensitivity, enough to see the traces of H I in molecular cloud cores, plus cold atomic gas in H I envelopes around the cores, will be applied to most of the Galactic disk, enabling comprehensive population studies of H_2 -forming clouds, including their proximity to spiral shocks (Minter et al. 2001; Gibson et al. 2005). GASKAP HISA will offer a rich new database for rigorous tests of theoretical models of gas-phase evolution in spiral arms (Dobbs & Bonnell 2007; Kim et al. 2008) including phase lags between spiral shocks and star formation (e.g. Tamburro et al. 2008). On much smaller scales, the turbulent froth of HISA filaments that appear to be pure cold H I will be revealed at threefold finer angular and velocity resolution in GASKAP than in all prior surveys, with sufficiently improved sensitivity to follow their spatial power spectrum down to subparsec scales. This investigation will relate clouds' turbulent support to their stage of molecular condensation. Both 21-cm continuum absorption and self-absorption toward Galactic objects, including masers, are

helpful for distance determinations (e.g. Anderson & Bania 2009; Green & McClure-Griffiths 2011).

3.6 Diffuse Molecular Clouds Traced by Extended OH Emission

In addition to H I spectroscopy, GASKAP will further enhance the exploration of gas-phase evolution with a new view of molecular clouds. The OH λ 18-cm lines have long been used as an alternative to the standard CO proxy for H₂, which is subject to the vagaries of ultraviolet shielding, interstellar chemistry, and sub-thermal excitation at densities below 10³ cm⁻³ (Liszt & Lucas 1996, 1999; Grenier et al. 2005; Sheffer et al. 2008; Wolfire et al. 2010). However, diffuse OH emission is typically about 100 times fainter than the H I 21-cm line, and there have been no large-area OH surveys since the ambitious survey of Turner (1979) with the Green Bank 43-m telescope. ASKAP's new capabilities bring an unbiased and detailed view of the OH sky within reach at last. By simultaneously mapping cold H I self-absorption at 20–60 arcsec resolution and diffuse OH at 90–180 arcsec resolution (to achieve the necessary brightness sensitivity), GASKAP will directly probe the H₂ formation process by providing a comprehensive H I + OH database of diffuse molecular clouds. These data can be compared to quiescent evolutionary models (e.g. Goldsmith et al. 2007; Liszt 2007) and converging-flow dynamical models (e.g. Bergin et al. 2004; Vázquez-Semadeni et al. 2007) to address a key question in the field: *How long do H₂ clouds take to form from the diffuse ISM, and how does this affect star formation?*

Measurement of cloud total column density, temperature, mass, and other properties will be needed to interpret millimeter-wave molecular line surveys, IR dust emission surveys, and other future Galactic observations. Of particular interest would be a broad-based analysis of cold H I, OH, CO, and dust in diffuse clouds throughout the Galaxy to establish a common evolutionary clock for clouds seen with multiple tracers. GASKAP's 3 σ OH 1667-MHz sensitivity translates to a minimum detectable H₂ column of $\sim 1.0 \times 10^{21}$ cm⁻² for a 2 km s⁻¹ wide line at 180-arcsec resolution, which is sufficient to sample the molecular content of an $A_V \sim 0.6$ mag diffuse molecular cloud, or the early OH formation in a dense molecular cloud. This sensitivity will exceed that reached by Turner (1979) with better velocity sampling and with angular resolution an order of magnitude sharper over a larger and unbiased area, including the hitherto unexplored fourth Galactic quadrant. At the same time, OH absorption toward continuum sources will be probed along with H I absorption to show the excitation temperatures of the 18-cm mainlines. Assuming optical depths of a few times 10⁻³ (Liszt & Lucas 1996) and rms noise of 1 mJy for a velocity resolution of 1 km s⁻¹ (Table 2), then background sources brighter than about 1 Jy will show detectable absorption in OH. Counting only extragalactic radio sources, there is one with flux den-

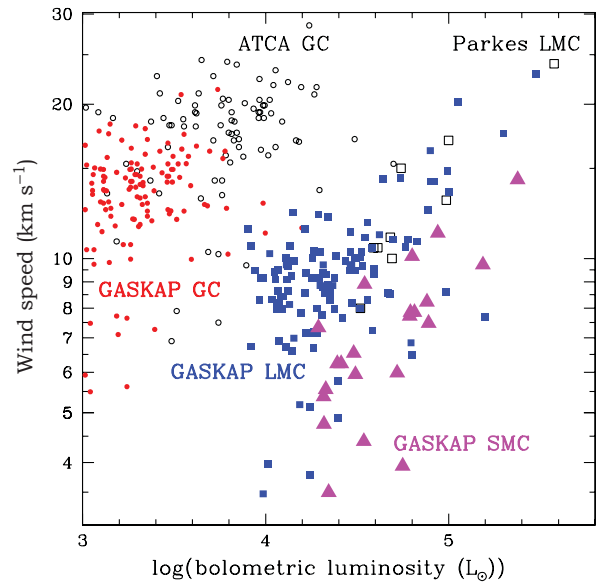


Figure 6. Expected distributions of OH masers in AGB stars and red supergiants based on empirical scaling relations in Marshall et al. (2004). Open symbols are known masers, with circles for the Galactic Center region and squares for the LMC; filled symbols are predictions for GASKAP detections, with triangles for SMC masers.

sity greater than 1 Jy at 1.4 GHz on average every 18 deg², but in the Galactic plane there will be many more H II regions and supernova remnants with flux densities well above 1 Jy, up to several per degree of longitude for $|\ell| < 25^\circ$. Thus, we expect many OH absorption spectra for comparison with H I absorption.

3.7 OH Masers in Young and Evolved Stars

OH masers allow us to study stellar birth and death, and give a picture of Galactic structure and dynamics complementary to that shown by the interstellar gas. The OH portion of the GASKAP survey will allow study of the sites of high-mass star formation and the old stars such as AGB stars, central stars of young PNe, and red supergiants that exhibit copious gas ejection in the last stages of their evolution. This phase of stellar evolution is a critical contributor to the chemical enrichment of the ISM. OH maser spectra enable us to study the energetics of outflows from massive young stellar objects (YSOs) and the mass-loss rates of dying stars by combining the measured radial velocities with estimates of the gas density in and around the OH emission region. With a sensitivity at least one order of magnitude better than previous spatially limited surveys of OH masers (e.g. Caswell & Haynes 1987; Sevenster et al. 2001), and taking into account the number of known OH maser sources to date (~ 2300 in evolved stars; Engels, Bunzel, & Heidmann 2010), we expect to find several thousand new OH maser sources (Figure 6). Such a sensitive and unbiased survey will allow us to make statistical studies of the processes in these evolutionary phases as well as proper comparisons with results of Galactic surveys at other

wavelengths. The total number of OH maser sources is also helpful in estimating the net mass ejection rate from stars in the Galaxy and in understanding the circulation of processed material back into the ISM.

The accuracy of the point-source position measurement is $\sigma_\theta \simeq \theta/[2(S/N)]$, where $\theta = \theta_s$ is the FWHM of the synthesised beam, and S/N is the signal-to-noise ratio of the source (e.g. Reid et al. 1988). For strong maser emission (>0.5 Jy) with spatial-velocity structure, subarcsecond velocity gradients will be measurable by finding the centroid of the emission in each velocity channel. This will allow the tracing of kinematic structures such as disks or outflows in some OH maser stars, including highly collimated jets and ‘super winds’ in some objects (Sahai et al. 1999; Cohen et al. 2006). GASKAP will allow us to obtain a complete catalogue of evolved stars in special transition phases, of which there are only a few members known so far. Zijlstra et al. (1989) catalogue several examples of such evolved stars showing both radio continuum and OH maser emission, which could be extremely young PNe. Moreover, the shape of OH maser spectra can help identify stars just leaving the AGB phase, when their spectra depart from the typical double-peaked profile. An extreme example are those evolved objects undergoing highly collimated jets, such as ‘water fountains’ (Imai et al. 2007). These special types of objects are key to understanding the evolution and morphology of PNe.

Using the systemic velocities of masers in OH/IR stars, GASKAP will allow study of Galactic kinematics as traced by this stellar population with much more detail and spatial extent than previously (e.g. Baud et al. 1981; Sevenster et al. 1999). This will provide a picture of MW stellar dynamics that complements those from the gas and from the very different stellar populations that will be sampled by *GAIA* at optical wavelengths.

Interstellar masers are one of the most readily detected signposts of locations where high-mass stars are forming. Surveys for masers are able to detect high-mass star formation regions throughout the Galaxy (e.g. Green et al. 2009), and the number of detected masers suggests that all high-mass star formation regions go through a phase where they have associated masers. There are four different types of interstellar masers commonly observed in high-mass star formation regions — ground-state OH masers at 1665 and 1667 MHz, 22 GHz water masers, class II methanol masers (most commonly at 6.7 and 12.2 GHz) and class I methanol masers (most commonly at 36 and 44 GHz). In addition to the common maser transitions, which are often (but not always) very strong, some sources also show maser emission from excited state OH transitions and/or higher frequency methanol transitions. These rarer masers are invariably weaker than the common masers observed in the same source (e.g. Ellingsen et al. 2011). Studies of the pumping mechanism of the commonly observed star formation masers show that the observed transitions are less selective than some of the rarer maser transitions and are inverted over a wider range of physical conditions (e.g. Cragg, Sobolev, & Godfrey 2003). Never-

theless, the detection of a particular maser transition toward a region indicates the presence of a relatively narrow range of physical conditions in the vicinity. Ellingsen et al. (2007) suggest that the presence and absence of different maser transitions toward a region can be used as an evolutionary clock for the high-mass star formation process and proposed a time sequence involving all the common maser transitions. Recent studies of methanol and water masers have further refined and quantified the maser-based timeline (e.g. Breen et al. 2010a, 2010b; Ellingsen et al. 2011). The sensitive GASKAP study represents a unique opportunity to robustly test and refine the way that ground-state OH maser emission fits in the timeline.

OH masers are generally thought to arise later than water and class II methanol masers in the evolution of high-mass star formation regions, but to persist after water and class II methanol switch off (Forster & Caswell 1989; Breen et al. 2010b). Most OH masers in high-mass star formation regions are strongest in the 1665-MHz transition, with weaker 1667-MHz emission and no 1612- or 1720-MHz maser emission. There are, however, exceptions to this pattern (e.g. Caswell 1999; Argon, Reid, & Menten 2003) and GASKAP represents the best opportunity to determine if the currently known exceptions represent unusual objects or perhaps short-lived evolutionary phases. Caswell (1999) found that the majority of high-mass star formation regions with a 1612-MHz OH maser were not associated with class II methanol masers, suggesting that these are generally older, more evolved star formation regions. Argon et al. (2003) found weak (200-mJy peak) 1665- and 1667-MHz OH masers toward the edges of a bipolar outflow traced by water masers toward the Turner–Welsh object near W3(OH). The Turner–Welsh object is a protostar with a synchrotron jet which is too young, or not sufficiently massive, to have produced an H II region. So the Argon et al. discovery appears to show that some OH masers are associated with very different objects from the high-mass protostars which traditionally show strong ground-state OH maser emission. However, if the luminosity of the masers in the Turner–Welsh object is typical, then no previous OH maser survey would have been sensitive to this class of object over a significant volume of the Galaxy. With a 5σ detection limit in a 0.2 km s^{-1} spectral channel of approximately 10 mJy (for the low-latitude survey), it will be possible to determine what fraction of the water and class II methanol masers have associated OH masers with peak flux densities significantly less than 0.5 Jy and also to detect any weak OH masers which are not associated with other types of masers. Simultaneous observations of three of the four ground-state OH maser transitions, combined with a growing amount of existing data on class I and II methanol masers and water masers, will enable us to substantially refine and improve the maser-based evolutionary clock for high-mass star formation regions. The strong Zeeman splitting experienced by ground-state OH transitions means that many OH masers in star formation regions are highly (up to 100%) circularly polarised and can be used to measure the total magnetic field in the maser region. The spatial resolution of the GASKAP

survey, combined with the (typically) complex 1665-/1667-MHz spectra in high-mass star formation regions, means that in most cases follow-up observations, either of excited-state OH maser transitions at higher frequencies or at higher spatial resolution, will be required to reliably determine the magnetic field from the star formation regions, although in some cases it may be possible to infer this directly from the GASKAP data products.

3.8 Galactic Metabolism in Action in the Magellanic Clouds

GASKAP will provide maps of both MCs with a 20-arcsec beam, which is 3–5 times better than that of the seminal Australia Telescope Compact Array (ATCA)+Parkes HI maps of the LMC (1-arcmin beam; Kim et al. 2003) and the SMC (98-arcsec beam; Stanimirović et al. 1999), cf. Figure 5. The GASKAP maps will have better velocity resolution (0.2 km s^{-1} versus 1.65 km s^{-1} for the earlier maps), and they will have tenfold better sensitivity, $\sigma_T = 0.18 \text{ K}$ when smoothed to 1.65 km s^{-1} and a 1-arcmin beam, compared to $\sim 2 \text{ K}$ for the best existing survey data. The wide velocity range covered by the GASKAP maps will include all high-speed gas. Crucially, the GASKAP maps will match the resolution of the *Spitzer* SAGE survey maps at $70 \mu\text{m}$ (18 arcsec) and the *Herschel* HERITAGE maps at $160 \mu\text{m}$ (12 arcsec). At the MC distance (50–60 kpc), a resolution of ~ 20 arcsec gives a linear size of $\sim 5 \text{ pc}$, typical of supernova remnants and IR Dark Clouds. The improved resolution allows direct links to be established between the sources of stellar feedback and the ISM's response, as well as to locate cold atomic clouds in absorption or self-absorption that are lost in the bright extended emission in lower resolution data.

Two fundamental questions that GASKAP can answer about the gas in the MCs are how effectively star formation can drive gas out of dwarf irregular galaxies, and how differently star formation progresses in a low-metallicity environment (Krumholz et al. 2009). These are both critical issues for understanding the formation of galaxies, through hierarchical merging of progressively smaller galactic building blocks. Thus, the GASKAP data on the MW and MCs will contribute to a fundamental astrophysical understanding of the processes that dominate the epoch of galaxy formation. Specific issues related to these questions include how much of the gas driven out of the MCs into the Bridge and Stream will ultimately fall back to the MCs, how much will fall onto the MW disk, how much will blend into the hot halo, and how much will be lost from the system altogether. In its lowest resolution mode, GASKAP will have the sensitivity to finally map the high-velocity gas that is seen in absorption in front of much of the LMC (Lehner, Staveley-Smith & Howk 2009). This will also finally allow the determination of a reliable metallicity and settle the question of whether this is a chance coincidence of a foreground Galactic cloud or whether it represents an outflow from the LMC. GASKAP will provide hundreds of HI absorption spectra through the MCs; these

will measure the mixture of warm and cool atomic gas and the respective spatial distributions and kinematics of each phase. The lower metallicity of the ISM in the MCs will inhibit cooling in the medium. This effect has already been seen in absorption surveys that have been done with a few background sources (Dickey et al. 1994; Marx et al. 1997), but GASKAP will give a much higher density of lines of sight.

Simultaneously with the HI observations, we will cover the MCs for the first time with an unbiased, flux-limited survey in the OH lines. Previous OH observations were targeted and had worse sensitivity than GASKAP, finding only the very brightest sources. The GASKAP OH survey of the MCs will detect many more OH maser sources in star-forming regions. Previous OH maser observations of evolved stars in the MCs had rms sensitivities in excess of $\sim 10 \text{ mJy}$ per 0.2 km s^{-1} channel. GASKAP achieves a 10 times better sensitivity, yielding an expected two orders of magnitude more OH masers in the LMC (cf. Figure 12 in Marshall et al. 2004) and the first such samples in the metal-poor SMC. Large samples of masers in such low-metallicity populations of cool giant and supergiant stars will test theories of the driving mechanism of the winds through measurement of their speeds from the double-peaked OH 1612-MHz maser profile (Marshall et al. 2004; van Loon 2006).

3.9 The Magellanic Stream — A Template for Galaxy Fueling Processes

Our closest example of a flow of gas from outside a galaxy making its way through the halo toward the disk is the MS. GASKAP will survey about 5000 deg^2 of the MS, the MB, and the LA (Putman et al. 2003). After smoothing the data cubes to 3 arcmin, we will achieve a 3σ sensitivity limit of $N(\text{HI}) = 3.6 \times 10^{18} \text{ cm}^{-2}$ per 20 km s^{-1} channel. GASKAP's combination of angular resolution, sensitivity, and spatial coverage is superior to all previous surveys of the Magellanic System (e.g. Hulsbosch & Wakker 1988; Putman et al. 2003; Brüns et al. 2005; McClure-Griffiths et al. 2009).

Moving along the Stream from the MCs toward the Northern tip (near $\delta \sim +40^\circ$), the HI shows a wealth of small-scale structure down to the resolution limit of the existing surveys (3 arcmin with the Arecibo radio telescope; Stanimirović et al. 2008). It is not clear what drives the onset of this turbulent structure in the MS or in accreting flows in general. Various dynamical instabilities are expected to disrupt the MS (Bland-Hawthorn et al. 2007; Heitsch & Putman 2009). Each has a distinct signature in the density and velocity fields, so that the GASKAP data will measure their relative importance. Strong dynamical instabilities will lead to gas streamers and coherent structures, while thermal instabilities are expected to lead to fragmentation down to parsec and subparsec scales (Burkert & Lin 2000; Heitsch et al. 2008; Palotti et al. 2008). HI clouds re-forming in the MW halo will have compact morphology and small velocity gradients, contrary to the freshly stripped MS material that

is expected to have a head–tail morphology. These morphological and kinematic signatures are powerful diagnostics of the eroding agents essential for feeding the accreting material into the galaxy. Such studies require high spatial and velocity resolution; they are not possible with existing survey data.

GASKAP observations will provide, for the first time, the angular resolution and sensitivity needed to resolve the interface regions between MS/LA/MB clouds and the surrounding hot gas. The physics of these interfaces is key to understanding how neutral gas flows both in and out through the halo. The temperatures and sizes of these interfaces determine the importance of thermal conduction for the dissipation of a ‘fluff’ of small, neutral cloudlets. Measuring the rate of this process is essential for understanding gas accretion in galaxies in general. The heart of this study will be a confluence of GASKAP observations and numerical simulations for cloud evolution by Heitsch et al. (2008) and Bland-Hawthorn et al. (2007).

Recent studies suggest that the MS is $\sim 40\%$ longer than previously thought, and it contains several long filaments (Stanimirović et al. 2008; Westmeier & Koribalski 2008; Nidever et al. 2010). This extended filamentary structure is directly related to the history and evolution of the MS. Numerical simulations that consider only gravitational interactions between the MCs and the MW (e.g. Connors et al. 2006) can reproduce such multiple filaments. However, these simulations require two separate tidal encounters between the SMC, the LMC, and the MW that are inconsistent with one of several recent proper-motion measurements of the MCs (Piatek et al. 2008) and complementary orbit calculations (Bekki 2011; Besla et al. 2010; Diaz & Bekki 2011). Using the combination of spatial coverage and angular resolution provided by GASKAP, we will study the fine structure and kinematics, including the radial velocity gradients of individual MS filaments (Stanimirović et al. 2008). The results will discriminate among models of the orbital history of the MCs and the role of both the luminous and dark matter components of the MW halo (Diaz & Bekki 2012).

3.10 The Cool Neutral Medium and Star Formation in Low-Density Environments

The MB presents a sliding scale of column density decreasing as one moves from the SMC toward the LMC. Star formation is observed to happen at the SMC end but not near the LMC (Gordon et al. 2009; Harris 2007). Recent Arecibo and ATCA observations show the existence of a multiphase medium in the MS (Stanimirović et al. 2008). H I emission profiles show clear evidence for a warm and a cold component, at a distance of 60 kpc above the MW disk. Matthews et al. (2008) detect an H I absorption line in the MS, revealing a cool, neutral medium (CNM) core with a temperature of 70 K and H I column density of $2 \times 10^{20} \text{ cm}^{-2}$. Such a multiphase medium with cold cores is unexpected in an environment such as the MS, based on the theoretical constraints on cooling/heating processes in the MW halo (Wolfire et al. 1995). GASKAP

will reveal and resolve many more cold cores in both the MS and the MB, allowing us to investigate the nature of the CNM in tidal tails, and thus the possible conditions for the formation of molecules, and ultimately stars, in low-density environments (Heitsch et al. 2008; Bournaud et al. 2004; Schaye 2004).

4 SIMULATIONS, IMAGING, AND ALGORITHM TESTS

4.1 H I Imaging

Simulations and tests of the imaging pipeline are a significant part of the GASKAP design study process. GASKAP’s imaging requirements differ from the other ASKAP Survey Science Projects (SSPs) because H I, and perhaps OH, emission will fill the entire FoV on all angular scales from arcseconds up to many degrees. In addition to this large-scale diffuse emission, we expect to see strong continuum absorption. The combination of strongly absorbed point sources in the midst of large-scale diffuse emission presents an imaging challenge. The imaging pipeline is being tested both through simulations of the ASKAP telescope’s response to a modeled H I sky and by using the ASKAP imaging software, ASKAPSOFT, on real interferometric data from the ATCA.

Two sets of simulations of the ASKAP telescope’s response to a modeled sky have been produced so far. These simulations were performed by the CASS staff using expected arrangements of the pointing centres for individual beams and the nominal beam shapes. The GASKAP H I simulations have been based on a sky model constructed by scaling the pixel sizes from the GASS survey (McClure-Griffiths et al. 2009; Kalberla et al. 2010) to produce a model input cube covering $8^\circ \times 8^\circ$ with a native resolution of 10 arcsec. The first round of simulations produced spectral line cubes of $6^\circ \times 6^\circ$ with resolutions of 30, 60, 90, and 180 arcsec. The simulations showed clearly that deconvolution of the telescope beam (cleaning) is necessary to improve image quality at all resolutions. The simulations used multiscale clean (MSCLEAN; Wakker & Schwarz 1988; Cornwell 2008; Rau & Cornwell 2011) for deconvolution and this appeared to work well. For the H I emission, a combination with single-dish survey data is also necessary, since much of the overall sky brightness is in very extended components that are filtered out by the aperture synthesis process. A second simulation has now been produced, which includes H I absorption toward continuum sources. This simulation will be used not only to test the imaging pipeline but also to test our H I absorption extraction pipeline.

Two clean algorithms have been tested, specifically MSCLEAN and maximum entropy. Maximum entropy is a common algorithm for deconvolution of images with large-scale diffuse emission, such as GASKAP (see e.g. Staveley-Smith et al. 2003; Stil et al. 2006; McClure-Griffiths et al. 2005). Maximum entropy produces a positive image with a compressed range of pixel values. The compressed range of

pixels tends to produce a very smooth image and the positivity means that negative sources, as produced by H I absorption where the continuum has been subtracted, are not deconvolved. MS-CLEAN is based on the traditional Högbom (1974) version, but rather than working with point sources, the algorithm works with multiple Gaussians of specified scale sizes. Work by Cornwell (2008), Rich et al. (2008), and Rau & Cornwell (2011) has shown that MS-CLEAN is much more effective at recovering large-scale flux density than traditional Högbom CLEAN, but it is untested in cases where emission fills the entire FoV. MS-CLEAN is the default deconvolution algorithm in the ASKAPSOFT imaging pipeline.

Working with existing H I data from the SGPS Galactic Center survey (McClure-Griffiths et al. 2012), we have compared the results of maximum entropy and MS-CLEAN. These tests indicated that MS-CLEAN gave qualitatively similar results to maximum entropy, with the added advantage that MS-CLEAN can deconvolve the absorbed continuum sources, whereas maximum entropy cannot. Furthermore, the compressed pixel range of maximum entropy means that the contrast between features in the images is often better with MS-CLEAN than with maximum entropy.

The GASKAP design study will determine the best method for combining H I single-dish data with the ASKAP interferometric data. A discussion of various techniques for this combination is presented by Stanimirović (2002). This topic has become top priority now that MS-CLEAN has been shown to be a viable deconvolution algorithm. The goal is to determine the most efficient and effective combination method, by exploring two options: combination with single-dish data during deconvolution, by giving the single-dish data as a model, and post-deconvolution combination, by ‘feathering’ the two images in the Fourier domain.

4.2 Synthetic Data Cubes with OH Maser Emission

One of the targets for GASKAP is the detection of Galactic OH masers, in the transitions at 1612, 1665, and 1667 MHz. The satellite line at 1612 MHz preferentially traces emission from evolved stars undergoing mass loss. These are mostly stars on the AGB, but some red supergiants, post-AGB stars, and PNe are also OH emitters. The main-line transitions at 1665 and 1667 MHz are prominent in massive star-forming regions, but they can also be found in evolved stars. OH maser emission is spatially compact (typically less than 10^{14} cm) and spectrally narrow (with intrinsic linewidths of $\simeq 0.1$ – 1 km s $^{-1}$, below thermal linewidths). Therefore, these masers are ideal targets for source-finding algorithms.

Since GASKAP will detect more than 10^4 maser sources, accurate and reliable source finding is crucial for our science objectives. To test the capabilities of source-finding algorithms when dealing with prospective GASKAP maser data, two simulated data sets of OH sources have been generated to represent a single ASKAP FoV, one for star formation masers ($\simeq 200$ entries) and another for evolved stars ($\simeq 1$ 200 entries).

These two input catalogues were processed using MIRIAD routines, to create a FITS cube of the expected output from a single ASKAP field. The final cubes had 1536×1536 spatial pixels across a $6^\circ \times 6^\circ$ field. The spectral resolution was 1.1-kHz channels (equivalent to a velocity resolution of 0.2 km s $^{-1}$ at the 1665-MHz frequency). There were 750 and 4000 spectral channels for the cubes of star formation and evolved objects, respectively. Maser features were assumed to be spatially unresolved and to have Gaussian spectral profiles, with widths ranging from 0.2 to 5 km s $^{-1}$ (simulating different amounts of spectral blending). The beam size in the cubes is approximately 30 arcsec, with 10-arcsec pixels. They were created using robust weighting, applying a Gaussian taper to the visibilities to reduce the weight of the long ASKAP baselines. Arbitrary noise levels can be added to the simulated data. For our first simulations, we have assumed that the data came from a single observing track of 10 h of integration time per pointing.

4.2.1 Simulated Catalogue of OH Masers in Evolved Stars

We have constructed a simulated ASKAP observing field at 1612 MHz around the Galactic Center. This region is the most crowded one in terms of OH-emitting evolved sources and, therefore, it is used as the most challenging scenario to test the efficiency of source-finding algorithms and study issues such as confusion and dynamic range limitations, considering that some OH masers can reach flux densities of hundreds of Jy.

As of 2010 July, the Engels et al. (2010) database listed 344 known stellar OH masers at 1612 MHz within 3° from the Galactic Center. A histogram of their flux densities is shown in Figure 7(a). However, this database is obviously incomplete for weak masers, since no large-scale survey has ever been conducted down to the sensitivities that can be reached with ASKAP. To estimate the total number of sources we can expect to detect in this field, we assumed that the actual flux density distribution of OH masers is similar to that obtained by Sjouwerman et al. (1998) in a smaller area (37×37 arcmin 2) around the Galactic Center, after correcting by their estimated completeness. We also assumed that the Engels database is complete for the strongest masers [$\log S_\nu$ (mJy) ≥ 2.5]. Under these assumptions, we obtained a total estimate of $\simeq 669$ sources with $S_\nu \geq 3$ mJy (Figure 7 b) within 3° from the Galactic Center. We note that the number of known stellar OH masers at 1612 MHz in this area is only about half of our estimated number, which indicates the usefulness of the sensitive and complete GASKAP survey of this type of sources. To calculate the possible spatial, flux density, and velocity distribution of the ‘still undetected’ sources, we considered some observational properties of the known OH masers, such as their usual association with SiO maser emission in AGB stars, and their mid-IR fluxes.

We considered as possible new sites of OH emission the known SiO masers without detected OH emission. The OH flux density was chosen to be increasing with the Midcourse

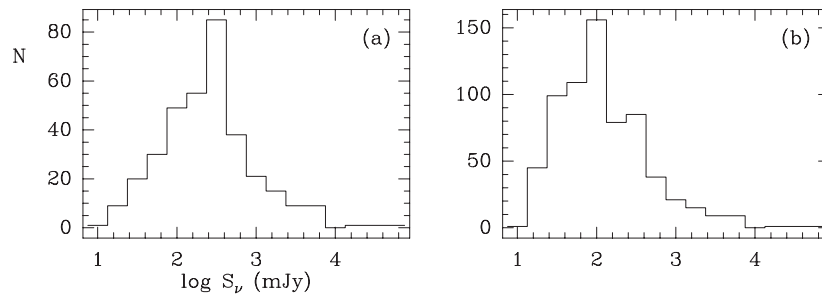


Figure 7. OH maser flux density distribution functions. (a) The flux density distribution of 344 known OH masers within 3° of the Galactic Center (catalogued in Engels et al. 2010). (b) The estimated flux density distribution of the expected sources in the same region, after correcting for completeness.

Space Experiment (MSX) flux density at $21 \mu\text{m}$, and conforming to the flux density distribution in Figure 1. The stellar velocities were directly derived from the SiO spectra and the OH masers were assumed to have a double-peaked shape, i.e. modeled as two Gaussians, with a velocity separation of 15 km s^{-1} (typical of AGB stars). The known OH maser sources plus these prospective sources selected from SiO maser sites amounted to a total of 556 sources. To complete the catalogue up to the expected 669 sources in the field, we selected the 83 brightest MSX sources fulfilling the mid-IR color characteristics typical of AGB stars (Sevenster 2002), and without known OH and SiO masers.

4.2.2 Simulated Catalogue of OH Masers in Star-Forming Sites

The star formation (1665 MHz) sample was derived from the 26 real sources located within a 6° -diameter field centered on 338° longitude (a region of the Galactic plane with a high level of star formation activity). It was supplemented with 15 extra (weak) sources based on extrapolating the best current estimate of the star formation OH luminosity function (Caswell & Haynes 1987) to the sensitivity limit of the GASKAP survey. The additional sources were located at the positions of the brightest 6.7-GHz methanol masers with so far undetected OH emission (from the Methanol Multibeam Survey; Green et al. 2009), for which the OH masers are known to have a close association with. In total, there were 195 features across 41 sources, including 60 features across the 15 newly generated sources. These results are illustrated in Figure 7.

5 DATA PRODUCTS

The primary GASKAP data product will be high spectral resolution ($\sim 0.2 \text{ km s}^{-1}$) cubes of the full survey region, covering H I emission over a velocity range of $\pm 760 \text{ km s}^{-1}$, 1612-MHz OH emission over $\pm 311 \text{ km s}^{-1}$, and the two OH maser lines at 1665 and 1667 MHz over $\pm 311 \text{ km s}^{-1}$. In addition to this, there will be two primary catalogues of spectra including OH maser emission and H I absorption against background continuum sources. Finally, there will also be high spatial resolution (2-arcsec pixels, 10-arcsec beam) postage

stamp cubes of all OH masers ($5 \times 5 \text{ arcmin}^2$) and H I and OH around all strong continuum sources ($60 \times 60 \text{ arcsec}^2$), thereby including all H I absorption features. Sensitivity maps and point spread function (PSF) maps spaced at suitable points will be provided so that the sensitivity and PSF can be interpolated to any point.

The data file size for a single image is anticipated to be 793 GB. This assumes that each FoV will be mapped out to dimensions of $7.5^\circ \times 7.5^\circ$, which will result in substantial overlap of fields (separated by 5°) and provide a significant guard band around the edges of each PAF FoV. On this basis, GASKAP will require approximately 1.0 PB of data storage space.

6 FOLLOW-UP SURVEYS

A complete survey of the MW disk requires combination of observations by telescopes in the Northern and Southern Hemispheres. For GASKAP, the natural complement is a survey with the Westerbork Synthesis Radio Telescope (WSRT) using the new array receiver Apertif (Verheijen et al. 2008). The proposed project, called the Galactic and Magellanic Emission Survey (GAMES), is intended to cover the remaining longitude range of the MW ($79^\circ < \ell < 167^\circ$) with the same latitude range and brightness sensitivity as GASKAP. The baseline distribution of the WSRT favors higher resolution, so GAMES may provide data products with better positional accuracy and finer detail than GASKAP, but the primary data product for GAMES will be spectral line cubes that are tapered to match in spatial and spectral resolution as closely as possible with GASKAP.

High-resolution follow-up on H I and OH continuum absorption and OH masers discovered by GASKAP will be possible using VLBI observations. ‘Tiny structures’ of H I clumps as absorption in front of extended continuum sources will supplement our knowledge of the power spectrum of the size distribution of H I clumps on scales down to 100 AU (Davis, Diamond, & Goss 1996; Deshpande 2000; Brogan et al. 2005). Similar absorption observations are possible for OH and H_2CO transitions at higher frequencies (e.g. Marscher, Moore, & Bania 1993). Similar VLBI observations of OH masers will reveal the details of the

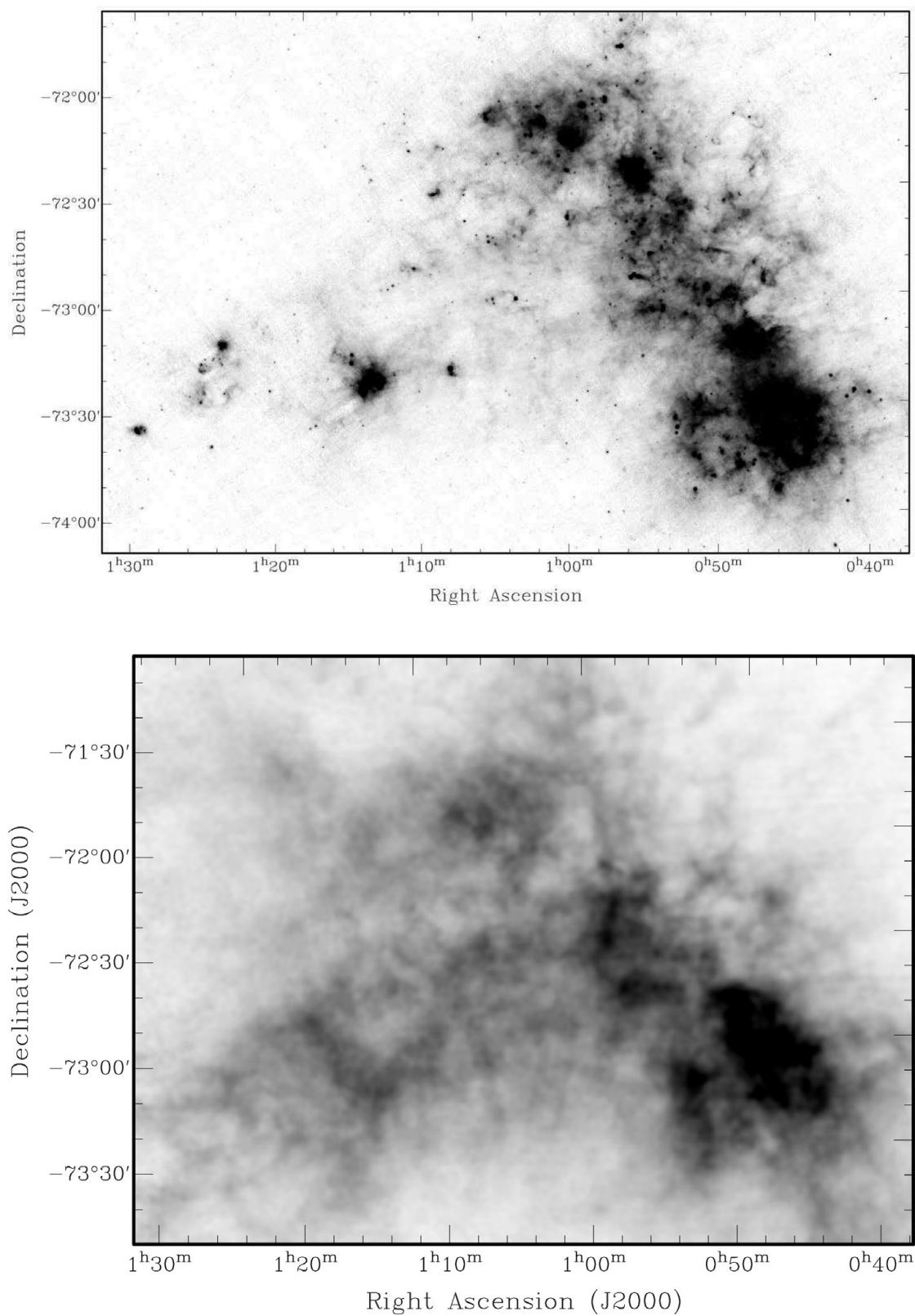


Figure 8. Two images of the SMC. On the top panel is the recent SAGE–SMC *Spitzer* Legacy image at 70 μm (Gordon et al. 2011) tracing dust emission in the far-IR with a resolution of 18 arcsec. The lower panel shows the best existing image in the 21-cm line, tracing total H I column density with a resolution of 1 arcmin (Stanimirović et al. 1999). The GASKAP survey will improve the resolution in the 21-cm line by a factor of 3, nearly matching the resolution of the *Spitzer* image.

spatial and kinematic structure of gas around YSOs and dying stars. VLBI astrometry of OH masers will provide an opportunity to study the dynamics of the MW as a whole. In contrast to recent maser astrometric observations that concentrate on star-forming regions in the Galactic thin disk (e.g. Reid et al. 2009), parallax and proper-motion observations of stellar OH masers may extend the exploration of MW dynamics to the Galactic thick disk. In the MCs, maser observations using VLBI astrometric techniques hold the promise of showing the proper motion and someday even the parallax of the Clouds. Additionally, full Stokes polarimetric observations of the OH masers with the ATCA, such as those being conducted for the MAGMO project (Green 2010), will enable exploration of the properties of the in situ magnetic field.

The GASKAP survey will be the most compelling scientific advertisement for the SKA because of its image quality. As an example of the value of comparing surveys of the ISM using different tracers, and also as an illustration of the power of imagery with high spatial resolution and dynamic range, Figure 8 shows two views of the SMC. In the top panel is an image of the dust made with data from *Spitzer* at 70- μm wavelength (Gordon et al. 2011) and in the lower panel is the best current image of the 21-cm column density of H I (Stanimirović et al. 1999). Far-IR dust maps and atomic hydrogen maps can be combined to estimate the amount and distribution of *molecular* gas, which is most directly associated with the star formation process (e.g. Bolatto et al. 2011), but for this to be accurate these maps need to have comparable angular resolution. The results of previous Galactic surveys demonstrate that GASKAP will produce images of structures in the ISM with stunning detail and compelling aesthetic appeal. For the general public, these images may be the most appealing results to come from the entire ASKAP effort. The GASKAP survey is designed to have the maximum possible impact to further the SKA project. The results will appeal to astronomers and non-astronomers and contribute to fields of study in a broad base of theoretical and observational research well beyond the traditional radio astronomy community.

7 SUMMARY

The GASKAP survey is the only approved survey science project for the ASKAP telescope that will concentrate on spectroscopy of the MW and Magellanic System with narrow velocity channels covering the H I and OH lines at wavelengths of 21 and 18 cm. Because it is the only such survey, GASKAP necessarily represents a combination of many different scientific applications and objectives. The results of the survey will be valuable for questions in cosmology, galaxy mergers and accretion, the structure and dynamics of the MCs and Stream, and of the outer halo of the MW through which they move. The survey will discover and catalogue thousands of OH masers, tracing outflows from evolved stars, as well as star formation regions and high-mass protostars. The MW ISM will be studied through different tracers that

show different thermal phases. One of the most difficult to study in any other way is the cool, atomic medium that will appear in absorption toward background continuum sources and sometimes toward the H I emission itself. The survey team includes specialists in all these topics and more, but the data will be made public as soon as their quality is assured. There is no proprietary period for the results of the survey, and archiving and distribution of preliminary survey data will begin long before the observations are finished.

The ASKAP project timetable depends on technical and administrative issues. As of late 2012, a small subset of the antennas, the Boolardy Engineering Test Array (BETA), is making test observations. By early 2014 a 12 antenna array will be taking scientific test data, including the first GASKAP survey fields. Recent single-dish and interferometer tests of the PAF on two 12-m dishes have been very encouraging, and the BETA array will soon be making aperture synthesis maps of test fields in various environments, including Galactic plane H I. Meanwhile computer simulations of the telescope response and resulting spectral line cubes are under intense study by members of the GASKAP team for planning purposes, particularly in source finding (continuum and OH masers), survey strategy, beam deconvolution, and data quality assurance.

REFERENCES

- Anderson, L. D., & Bania, T. M. 2009, *ApJ*, 690, 706
 Argon, A. L., Reid, M. J., & Menten, K. M. 2003, *ApJ*, 593, 925
 Baud, B., Habing, H. J., Matthews, H. E., & Winnberg, A. 1981, *A&A*, 95, 156
 Breen, S. L., Caswell, J. L., Ellingsen, S. P., & Phillips, C. J. 2010a, *MNRAS*, 406, 1487
 Breen, S. L., Ellingsen, S. P., Caswell, J. L., & Lewis, B. E. 2010b, *MNRAS*, 401, 2219
 Bekki, K. 2011, *MNRAS*, 416, 2359
 Bergin, E. A., Hartmann, L. W., Raymond, J. C., & Ballesteros-Paredes, J. 2004, *ApJ*, 612, 921
 Besla, G., Kallivayalil, N., Hernquist, L., van der Marel, R. P., Cox, T. J., & Kereš, D. 2010, *ApJ*, 721, 97
 Bland-Hawthorn, J., Sutherland, R., Agertz, O., & Moore, B. 2007, *ApJ*, 670, 109
 Bland-Hawthorn, J., Veilleux, S., Cecil, G. N., Putman, M. E., Gibson, B. K., & Maloney, P. R. 1998, *MNRAS*, 299, 611
 Bolatto, A. D., et al. 2011, *ApJ*, 741, 12
 Bournaud, F., Duc, P.-A., Amram, P., Combes, F., & Gach, J.-L. 2004, *A&A*, 425, 813
 Brogan, C. L., Zauderer, B. A., Lazio, T. J., Goss, W. M., DePree, C. G., & Faison, M. D. 2005, *AJ*, 130, 698
 Brooks, A. M., Governato, F., Quinn, T., Brook, C. B., & Wadsley, J. 2009, *ApJ*, 694, 396
 Brüns, C., et al. 2005, *A&A*, 432, 45
 Burkert, A., & Lin, D. N. C. 2000, *ApJ*, 537, 270
 Caswell, J. L. 1999, *MNRAS*, 308, 683
 Caswell, J. L., & Haynes, R. F. 1987, *AuJPh*, 40, 215
 Chippendale, A., O'Sullivan, J., Reynolds, J., Gough, R., Hayman, D., & Hay, S. 2010, in *IEEE Symp. Phased Array Systems and Technology*, 648

- Cichowolski, S., Pineault, S., Arnal, E. M., & Cappa, C. E. 2008, *A&A*, 478, 443
- Cohen, R. J., Gasprong, N., Meaburn, J., & Graham, M. F. 2006, *MNRAS*, 367, 541
- Condon, J. J., & Mitchell, K. J. 1984, *AJ*, 89, 610
- Connors, T. W., Kawate, D., & Gibson, B. K. 2006, *MNRAS*, 371, 108
- Cornwell, T. J. 2008, *J-STSP*, 2, 793
- Cragg, D. M., Sobolev, A. M., & Godfrey, P. D. 2002, *MNRAS*, 331, 521
- Crovisier, J., & Dickey, J. M. 1983, *A&A*, 122, 282
- Dalgarno, A., & McCray, R. A. 1972, *ARA&A*, 10, 375
- Davis, R. J., Diamond, P. J., & Goss, W. M. 1996, *MNRAS*, 283, 1105
- Dawson, J. R., McClure-Griffiths, N. M., Dickey, J. M., & Fukui, Y. 2011a, *ApJ*, 741, 85
- Dawson, J. R., McClure-Griffiths, N. M., Kawamura, A., Mizuno, N., Onishi, T., Mizuno, A., & Fukui, Y. 2011b, *ApJ*, 728, 127
- Deshpande, A. A. 2000, *MNRAS*, 317, 199
- Diaz, J., & Bekki, K. 2011, *PASA*, 28, 117
- Diaz, J., & Bekki, K. 2012, *ApJ*, 750, 36
- Dickey, J. M., McClure-Griffiths, N. M., Stanimirović, S., Gaensler, B. M., & Green, A. J. 2001, *ApJ*, 561, 264
- Dickey, J. M., Mebold, U., Marx, M., Amy, S., Haynes, R. F., & Wilson, W. 1994, *A&A*, 289, 357
- Dickey, J. M., Mebold, U., Stanimirović, S., & Staveley-Smith, L. 2000, *ApJ*, 536, 756
- Dobbs, C. L., & Bonnell, I. 2007, *MNRAS*, 376, 1747
- Ellingsen, S. P., Breen, S. L., Sobolev, A. M., Voronkov, M. A., Caswell, J. L., & Lo, N. 2011, *ApJ*, 742, 109
- Ellingsen, S. P., Voronkov, M. A., Cragg, D. M., Sobolev, A. M., Breen, S. L., & Godfrey, P. D. 2007, in *Proc. IAU Symp. 242, Astrophysical Masers and Their Environments* ed. Chapman J. M. & Baan W. A. (Cambridge: Cambridge University Press), 213
- Engels, D., Bunzel, F., & Heidmann, B. 2010, *Database of Circumstellar Masers v2.0*, <http://www.hs.uni-hamburg.de/st2b102/maserdb/index.html>
- Field, G. B., Goldsmith, D. W., & Habing, H. J. 1969, *ApJ*, 155, L149
- Ford, H. A., Lockman, F. J., & McClure-Griffiths, N. M. 2010, *ApJ*, 722, 367
- Ford, H. A., McClure-Griffiths, N. M., Lockman, F. J., Bailin, J., Calabretta, M. R., Kalberla, P. M. W., Murphy, T., & Pisano, D. J. 2008, *ApJ*, 688, 290
- Forster, J. R., & Caswell, J. L. 1989, *A&A*, 213, 339
- Gibson, S. J. 2010, *ASPC*, 438, 111
- Gibson, S. J., Taylor, A. R., Higgs, L. A., Brunt, C. M., & Dewdney, P. E. 2005, *ApJ*, 626, 195
- Gibson, S. J., Taylor, A. R., Higgs, L. A., & Dewdney, P. E. 2000, *ApJ*, 540, 851
- Goldsmith, P. F. 2007, in *Exploring the Cosmic Frontier: Astrophysical Instruments for the 21st Century*, ed. A. P. Lobanov, J. A. Zensus, C. Cesarsky, & P. Diamond (Berlin: Springer), 209
- Goldsmith, P. F., Li, D., & Krčo, M. 2007, *ApJ*, 654, 273
- Gordon, K. D., et al. 2009, *ApJ*, 690, 76
- Gordon, K. D., et al. 2011, *AJ*, 142, 102
- Green, D. A. 1993, *MNRAS*, 262, 327
- Green, J. A. 2010, *ASPC*, 438, 38
- Green, J. A., & McClure-Griffiths, N. M. 2011, *MNRAS*, 417, 2500
- Green, J. A., et al. 2009, *MNRAS*, 392, 783
- Grenier, I. A., Casandjian, J.-M., & Terrier, R. 2005, *Sci*, 307, 1292
- Gupta, N., Johnston, S., & Feain, I. 2008, *ATNF SKA Memo Ser*, 016 (http://www.atnf.csiro.au/projects/askap/newdocs/ng_config.pdf)
- Harris, J. 2007, *ApJ*, 658, 345
- Haverkorn, M., Gaensler, B. M., Brown, J. C., Bizunok, N. S., McClure-Griffiths, N. M., Dickey, J. M., & Green, A. J. 2006, *ApJ*, 637, 33
- Heitsch, F., Hartmann, L. W., Slyz, A. D., Devriendt, J. E. G., & Burkert, A. 2008, *ApJ*, 674, 316
- Heitsch, F., & Putman, M. E. 2009, *ApJ*, 698, 1485
- Hennebelle, P., & Audit, E. 2007, *A&A*, 465, 431
- Hill, A. S., Haffner, L. M., & Reynolds, R. J. 2009, *ApJ*, 703, 1832
- Högbom, J. A. 1974, *A&AS*, 15, 417
- Hulsbosch, A., & Wakker, B. P. 1988, *A&AS*, 75, 191
- Imai, H., et al. 2007, *PASJ*, 59, 1107
- Jenkins, E. B., & Tripp, T. M. 2011, *ApJ*, 734, 65
- Johnston, S., & Gray, A. 2006, *SKA Memo Ser.*, 72
- Johnston, S., et al. 2007, *PASA*, 24, 174
- Johnston, S., et al. 2008, *ExA*, 22, 151
- Kalberla, P. M. W., Burton, W. B., Hartmann, D., Arnal, E. M., Bajaja, E., Morras, R., & Pöppel, W. G. L. 2005, *A&A*, 440, 767
- Kalberla, P. M. W., et al. 2010, *A&A*, 521, 17
- Kang, J.-h., & Koo, B.-C. 2007, *ApJS*, 173, 85
- Kavars, D. W., Dickey, J. M., McClure-Griffiths, N. M., Gaensler, B. M., & Green, A. J. 2005, *ApJ*, 626, 887
- Kerp, J., Winkel, B. Ben Bekhti, N., Flöer, L., & Kalberla, P. M. W. 2011, *AN*, 332, 637
- Kerton, C. R., Knee, L. B. G., & Schaeffer, A. J. 2006, *AJ*, 131, 1501
- Kilborn, V. A., et al. 2000, *AJ*, 120, 1342
- Kim, C.-G., Kim, W.-T., & Ostriker, E. C. 2008, *ApJ*, 681, 1148
- Kim, S., Staveley-Smith, L., Dopita, M. A., Sault, R. J., Freeman, K. C., Lee, Y., & Chu, Y.-H. 2003, *ApJS*, 148, 473
- Klaassen, P. D., Plume, R., Gibson, S. J., Taylor, A. R., & Brunt, C. M. 2005, *ApJ*, 631, 1001
- Krčo, M., Goldsmith, P. F., Brown, R. L., & Li, D. 2008, *ApJ*, 689, 276
- Krumholz, M. R., McKee, C. F., & Tumlinson, J. 2009, *ApJ*, 699, 850
- Lazarian, A., & Pogosyan, D. 2000, *ApJ*, 537, 720
- Lazarian, A., & Pogosyan, D. 2006, *ApJ*, 652, 1348
- Lehner, N., Staveley-Smith, L., & Howk, J. C., 2009, *ApJ*, 702, 840
- Libert, Y., Gérard, E., & Le Bertre, T. 2007, *MNRAS*, 380, 1161
- Liszt, H. 2007, *A&A*, 461, 205
- Liszt, H., & Lucas, R. 1996, *A&A*, 314, 917
- Liszt, H., & Lucas, R. 1999, *ASPC*, 156, 188
- Lockman, F. J. 2002, *ApJ*, 580, 47L
- Lockman, F. J., Benjamin, R. A., Heroux, A. J., & Langston, G. I. 2008, *ApJ*, 679, L21
- Maller, A. H., & Bullock, J. S. 2004, *MNRAS*, 355, 694
- Marasco, A., Fraternali, F., & Binney, J. J. 2012, *MNRAS*, 419, 1107
- Marscher, A. P., Moore, E. M., & Bania, T. M. 1993, *ApJ*, 419, L401
- Marshall, J. R., van Loon, J. Th., Matsuura, M., Wood, P. R., Zijlstra, A. A., & Whitelock, P. A. 2004, *MNRAS*, 355, 1348
- Marx, M., Dickey, J. M., & Mebold, U. 1997, *A&AS*, 126, 325

- Matthews, L. D., Libert, Y., G' erard, E. Le Bertre T., & Reid, M. J. 2008, *ApJ*, 684, 603
- McClure-Griffiths, N. M. 2009, *ApJS*, 181, 398
- McClure-Griffiths, N. M., Dickey, J. M., Gaensler, B. M., & Green, A. J. 2003, *ApJ*, 594, 833
- McClure-Griffiths, N. M., Dickey, J. M., Gaensler, B. M., & Green, A. J. 2004, *ApJ*, 607, 127
- McClure-Griffiths, N. M., Dickey, J. M., Gaensler, B. M., Green, A. J., Green, J. A., & Haverkorn, M. 2012, *ApJ.Supp.*, 199, 12
- McClure-Griffiths, N. M., Dickey, J. M., Gaensler, B. M., Green, A. J., Haverkorn, M., & Strasser, S. 2005, *ApJS*, 158, 178
- McClure-Griffiths, N. M., et al. 2006, *ApJ*, 638, 196
- Minter, A. H., Lockman, F. J., Langston, G. I., & Lockman, J. A. 2001, *ApJ*, 555, 868
- Miszalski, B., Parker, Q. A., Acker, A., Birkby, J. L., Frew, D. J., & Kovacevic, A. 2008, *MNRAS*, 384, 525
- Momjian, E., & Perley, R. 2011, NRAO EVLA Memo, 152 (<http://www.aoc.nrao.edu/evla/geninfo/memoseries/evlamemo152.pdf>)
- Muller, E. Stanimirovi'c, S., Rosolowsky, E., & Staveley-Smith, L. 2004, *ApJ*, 616, 845
- Nidever, D. L., Majewski, S. R., & Burton, W. B. 2008, *ApJ*, 679, 432
- Nidever, D. L., Majewski, S. R., Burton, W. B., & Nigra, L. 2010, *ApJ*, 723, 1618
- Normandeau, M., Taylor, A. R., & Dewdney, P. E. 1996, *Natur*, 380, 687
- Olano, C. A. 2008, *A&A*, 485, 457
- Olsen, K. A., Zaritsky, D., Blum, R. D., Boyer, M. L., & Gordon, K. D. 2011, *ApJ*, 737, 29
- Palotti, M. L., Heitsch, F., Zweibel, E. G., & Huang, Y.-M. 2008, *ApJ*, 678, 234
- Peek, J. E. G., et al. 2011a, *ApJS*, 194, 20
- Peek, J. E. G., Heiles, C., Peek, K. M. G., Meyer, D. M., & Lautoesch, J. T. 2011b, *ApJ*, 735, 129
- Peek, J. E. G., Putman, M. E., McKee, C. F., Heiles, C., & Stanimirovi'c, S. 2007, *ApJ*, 656, 907
- Petrov, L., Hirota, T., Honma, M., Shibata, K. M., Jike, T., & Kobayashi, H. 2007, *AJ*, 133, 2487
- Piatek, S., Pryor, C., & Olszewski, E. W. 2008, *AJ*, 135, 1024
- Pidopryhora, Y., Lockman, F. J., & Rupen, M. P. 2009, in *The Role of Disk–Halo Interaction in Galaxy Evolution: Outflow vs. Infall?*, ed. M. A. de Avillez (Les Ulis: European Astronomical Society Publications Series)
- Putman, M. E., Saul, D. R., & Mets, E. 2011, *MNRAS*, 586, 170
- Putman, M. E., Staveley-Smith, L., Freeman, K. C., Gibson, B. K., & Barnes, D. G. 2003, *ApJ*, 586, 170
- Putman, M. E., et al. 2009, *Astro 2010: The Astronomy and Astrophysics Decadal Survey*, Science White Papers, no. 241
- Rau, U., & Cornwell, T. J. 2011, *A&A*, 532, 71
- Reid, M. J., Schneps, M. H., Moran, J. M., Gwinn, C. R., Genzel, R., Downes, D., & Roennaeng, B. 1988, *ApJ*, 330, 809
- Reid, M. J., et al. 2009, *ApJ*, 700, 137
- Rich, J. W., de Blok, W. J. G., Cornwell, T. J., Brinks, E., Walter, F., Bagetakos, I., & Kennicutt, R. C. Jr, 2008, *AJ*, 136, 2897
- Sahai, R., te Lintel Hekkert, P., Morris, M., Zijlstra, A., & Likkell, L. 1999, *ApJ*, 514, 115
- Schaye, J. 2004, *ApJ*, 609, 667
- Sevenster, M. N. 2002, *AJ*, 123, 2772
- Sevenster, M., Saha, P., Valls-Gabaud, D., & Fux, R. 1999, *MNRAS*, 307, 584
- Sevenster, M., van Langevelde, H. J., Moody, R. A., Chapman, J. M., Habing, H. J., & Killeen, N. E. B. 2001, *A&A*, 366, 481
- Sheffer, Y., Rogers, M., Federman, S. R., Abel, N. P., Gredel, R., Lambert, D. L., & Shaw, G. 2008, *ApJ*, 687, 1075
- Sjouwerman, L. O., van Langevelde, H. J., Winnberg, A., & Habing, H. J. 1998, *A&AS*, 128, 35
- Stanimirovi'c, S. 2002, *ASPC*, 278, 375
- Stanimirovi'c, S. 2010, Proc. ISKAF2010 Science Meeting, 2010 June 10–14, Assen, the Netherlands, 52
- Stanimirovi'c, S., Hoffman, S., Heiles, C., Douglas, K. A., Putman, M., & Peek, J. E. G. 2008, *ApJ*, 680, 276
- Stanimirovi'c, S., & Lazarian, A. 2001, *ApJ*, 551, 53
- Stanimirovi'c, S., Staveley-Smith, L., Dickey, J. M., Sault, R. J., & Snowden, S. L. 1999, *MNRAS*, 302, 417
- Stanimirovi'c, S., et al. 2006, *ApJ*, 653, 1210
- Staveley-Smith, L., Kim, S., Calabretta, M. R., Haynes, R. F., & Kesteven, M. J. 2003, *MNRAS*, 339, 87
- Stil, J. M., Taylor, A. R., Martin, P. G., Rothwell, T. A., Dickey, J. M., & McClure-Griffiths, N. M. 2004, *ApJ*, 608, 297
- Stil, J. M., et al. 2006, *AJ*, 132, 1158
- Strasser, S. T., et al. 2007, *AJ*, 134, 2252
- Tamburro, D., Rix, H.-W., Walter, F., Brinks, E., de Blok, W. J. G., Kennicutt, R. C., & Mac Low, M.-M. 2008, *AJ*, 136, 2872
- Tasker, E. J., Brunino, R., Mitchell, N. L., Michielsen, D., Hopton, S., Pearch, F. R., Bryan, G. L., & Theuns, T. 2008, *MNRAS*, 390, 1267
- Taylor, A. R., et al. 2003 *AJ*, 125, 3145
- Tonnesen, S., & Bryan, G. L. 2009, *ApJ*, 694, 789
- Turner, B. E. 1979, *A&A*, 37, 1
- van Loon, J. Th. 2006, *ASPC*, 353, 211
- Vázquez-Semadeni, E., Gómez, G. C., Jappsen, A. K., Ballesteros-Paredes, J. González, R. F., & Klessen, R. S. 2007, *ApJ*, 657, 870
- Vázquez-Semadeni, E., Ryu, D., Passot, T., González, R. F., & Gazol, A. 2006, *ApJ*, 643, 245
- Verheijen, M. A. W., Oosterloo, T. A., van Cappellen, W. A., Bakker, L., Ivashina, M. V., & van der Hulst, J. M. 2008, *AIPC*, 1035, 265
- Wakker, B. P., & Schwarz, U. J. 1988, *A&A*, 200, 312
- Wakker, B. P., & van Woerden, H. 1991, *A&A*, 250, 509
- Westmeier, T., & Koribalski, B. S. 2008, *MNRAS*, 388, 29
- Wolfire, M. G., Hollenbach, D., McKee, C. F., Tielens, A. G. G. M., & Bakes, E. L. O. 1995, *ApJ*, 443, 152
- Wolfire, M. G., McKee, C. F., & Hollenbach, D. 2010, *ApJ*, 716, 1191
- Wolfire, M. G., McKee, C. F., Hollenbach, D., & Tielens, A. G. G. M. 2003, *ApJ*, 587, 278
- Zijlstra, A. A., te Lintel Hekkert, P., Pottasch, S. R., Caswell, J. L., Ratag, M., & Habing, H. J. 1989, *A&A*, 217, 157